9G45-24

PROJECT NERO
Nimbus Earth Resources Observations

Contract No. NAS 5-10343
Technical Report No. 7

Romeo R. Sabatini
John E. Sissala

ALLIED RESEARCH ASSOCIATES, INC.
Virginia Road, Concord, Massachusetts 01742

Prepared for

National Aeronautics and Space Administration
Goddard Space Flight Center
Greenbelt , Maryland

9G45-24

PROJECT NERO
Nimbus Earth Resources Observations

Contract No. NAS 5-10343
Technical Report No. 7

Romeo R. Sabatini
John E. Sissala

ALLIED RESEARCH ASSOCIATES, INC.
Virginia Road, Concord, Massachusetts 01742

Prepared for

National Aeronautics and Space Administration
Goddard Space Flight Center
Greenbelt , Maryland

ABSTRACT

This report is a survey of non-meteorological investigations completed with Nimbus photographic and infrared data. Only a minimal portion of the voluminous amounts of data have been analyzed for non-meteorological applications, and already the data have found applications in such fields as oceanography, geology, geography, and hydrology. The non-meteorological applications presented herein are definitively pertinent to the assessment of many proposed experiments for future Earth Resources satellites.

Section 2 lists and briefly comments on the studies accomplished with the television data (Advanced Vidicon Camera System and Automatic Picture Transmission).

Section 3 surveys the problems encountered in the use of the Nimbus High Resolution Infrared Radiation (HRIR) data and presents studies done with the HRIR and Medium Resolution Infrared Radiation (MRIR) data.

Section 4 summarizes the experiments on future Nimbus satellites and their application to the Earth Resources Program.

TABLE OF CONTENTS

TABLE OF CONTENTS (cont)

LIST OF FIGURES

LIST OF FIGURES (cont)

LIST OF TABLES

1. INTRODUCTION

The primary objective of the Nimbus satellites is to provide new and better meteorological observations from space. This task has been accomplished magnificently to date. The voluminous Nimbus data collected can also find ancillary applications in other branches of the earth sciences such as oceanography, geology, geography, hydrology, and therefore can be useful to the Earth Resources Program.

This report analyzes and presents examples of those non-meteorological applications of the Nimbus data relevant to the Earth Resources Program. Nimbus measurements of radiation and television pictures are obviously applicable to preliminary assessment studies, even though the resolutions are an order or two of magnitude less than the resolutions required by many proposed Earth Resources experiments (Ref. 1). Nimbus resolutions are at best of the order of 1, 2, 5, and 35 miles for the AVCS, APT, HRIR and MRIR systems respectively.

Table 1 lists the types of investigations feasible with the Nimbus I and II data and applicable to the solution or assessment of Earth Resources problems. The list, by no means exhaustive, has been compiled by selecting only those applications, limited by the Nimbus resolutions, which in our opinion have some merit. Meteorological applications of the data, which are covered extensively in the literature (Refs. 2 and 3), are not included, although they are of primary importance in the Earth Resources Program.

The use of AVCS and APT photography, and HRIR temperature maps involves pattern recognition and comparison to available topic maps. In the AVCS and APT the patterns are formed by shades attributable to the relative differences in reflection (albedo) of various surfaces. In the HRIR temperature maps, the patterns have more subtle significance when not related to terrain height differences or presence of clouds. Temperature anomalies may be attributed then to relative abundance of ground water, varying surface thermal property, water surfaces, vegetation surfaces, snow or ice, or a combination of any of these. Only through a judicious exclusion process can one determine the most likely cause for the temperature anomalies and their significance. This is at best difficult and sometimes impossible without some a priori knowledge of the terrain.

The MRIR data, because of their low resolution, are best applicable to mesoscale and worldwide heat budget calculations.

Section 2 examines the possible applications of AVCS and APT data. Section 3 does the same for HRIR and MRIR. Section 4 examines the possible applications of future Nimbus experiments.

Table 1

Types of Investigations Feasible with the Nimbus I and II Data
Applicable to the Solutions or Assessment of Earth Resources Problems

Type of Investigation	Applicable Sensors
1. Improvement of Topographic Base Maps	
a) Mapping of geomorphological features (faults, folds, basins, lineaments, etc.)	AVCS, APT, HRIR
b) Mapping of gross terrain and rock types such as igneous masses; calcareous deposits sand, etc.	AVCS, APT, HRIR
c) Vegetation vs. no Vegetation and seasonal variations	AVCS, APT, HRIR
d) Coastline determination	AVCS, APT
e) Possible areas of volcanic activity	HRIR
2. Oceanography and Limnology of Large Lakes	
a) Temperatures	HRIR
b) Currents, upwellings and sinkings	HRIR
c) Radiative terms of the energy budget	MRIR, HRIR
d) Distribution of ice cover	AVCS, APT, HRIR
e) Movement of sea ice	AVCS, APT
3. Hydrology	
a) Distribution of soil moisture	HRIR
b) Snow extent	AVCS, APT, HRIR
c) Basin geomorphology	AVCS, APT, HRIR
d) Areas inundated during a flood	AVCS, APT, HRIR
4. Energy Budget (Radiative Terms)	
a) Selected areas	MRIR, HRIR
b) World	MRIR, HRIR

2. NON-METEOROLOGICAL APPLICATIONS OF THE NIMBUS TV DATA

The advent of the TIROS series of meteorological satellites made available a new operational and research tool for the meteorological community. The resolution and sensitivity of the TIROS cameras were designed primarily for meteorological applications, however, the earth scientists were quick to realize some of the applications and benefits of these pictures. Among others, Wark and Popham (Refs. 4 and 5) demonstrated their usefulness in identifying ice phenomena. Tarble (Ref. 6) presented cases on the area distribution of snow as viewed from satellite photographs. Cronin (Ref. 7) mapped and described some of the large scale terrestrial features of the United States visible in the TIROS pictures. Merifield and Rammelkamp (Ref. 8) analyzed many desert area pictures for their geological significance. Morrison and Bird (Ref. 9) presented a summary of the non-meteorological applications and advantages of satellite photography.

With the launch of Nimbus I into an unplanned elliptical orbit with a perigee of about 223 nautical miles (423 km) earth scientists had nearly complete coverage of the earth's surface with improved TV resolution and sensitivity. Nimbus II TV data, although not of the high resolution or quality of Nimbus I because of a higher orbit (600 nautical miles) and a 10 kc interference pattern visible in the AVCS pictures, did provide full earth AVCS coverage for 4-1/2 months in 1966 and APT coverage from May 1966 to April 1968.

Research, to date, on Nimbus I and II AVCS and APT sensor photographs has demonstrated the utility and relevance of such satellite data for earth resource applications and research. The fields of geology, cartography, geography, hydrology and oceanography have benefited from these data. The following studies document some of the uses already made of the Nimbus photographs.

In one study (Ref. 10) a Nimbus I APT photograph of the Appalachian Mountains of Pennsylvania showed remarkable correlation with rock-type units as depicted by the 1:250,000 Geologic Map of Pennsylvania, published by the State Geological Survey (1960). A similar scale of structural geologic definition is revealed by a Nimbus I AVCS photograph of the Paris Basin in Central France (Ref. 11 and Figs. 1 and 2).

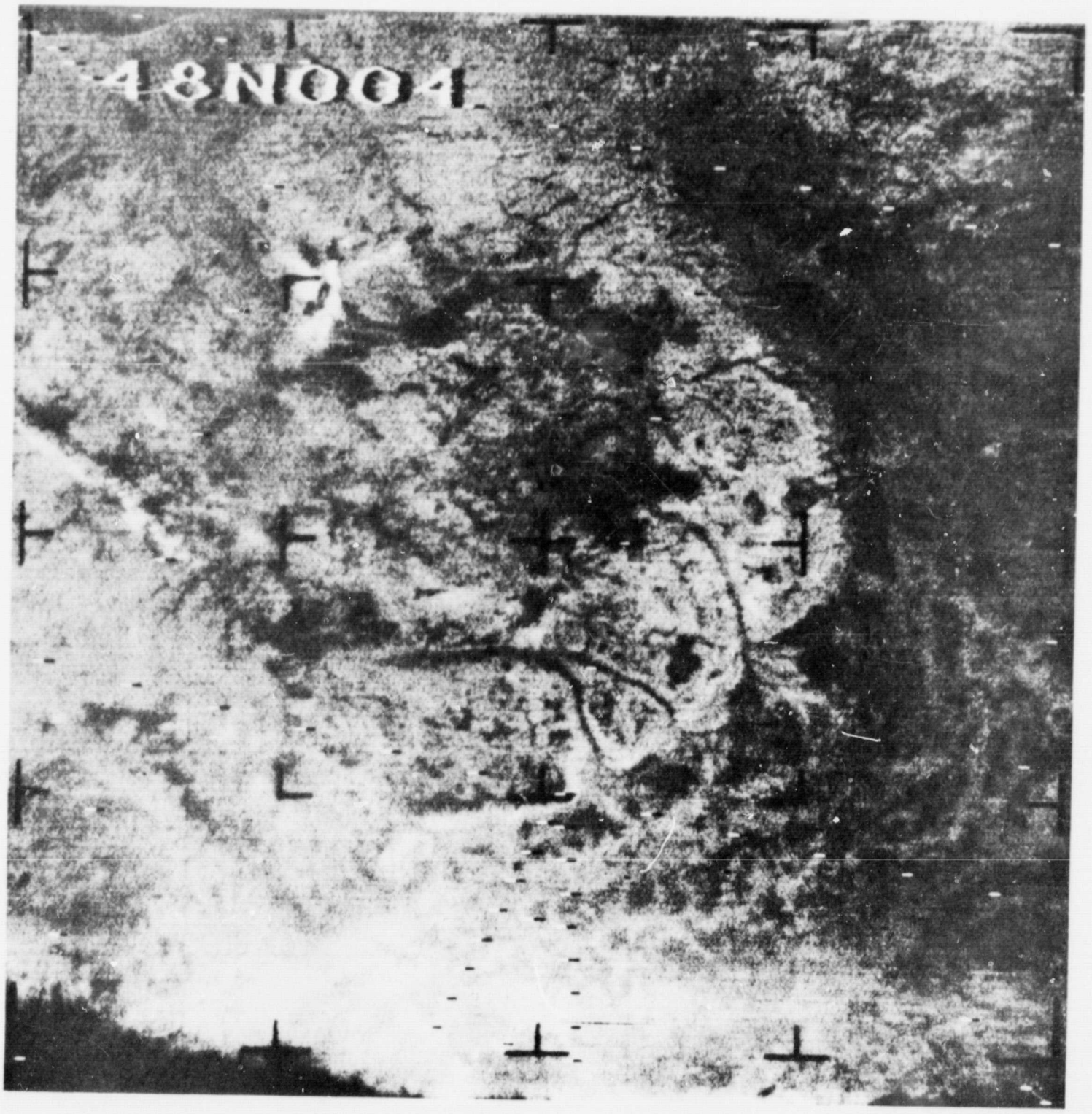

Figure 1 Nimbus I AVCS Picture of Paris Basin Geology in Central France.

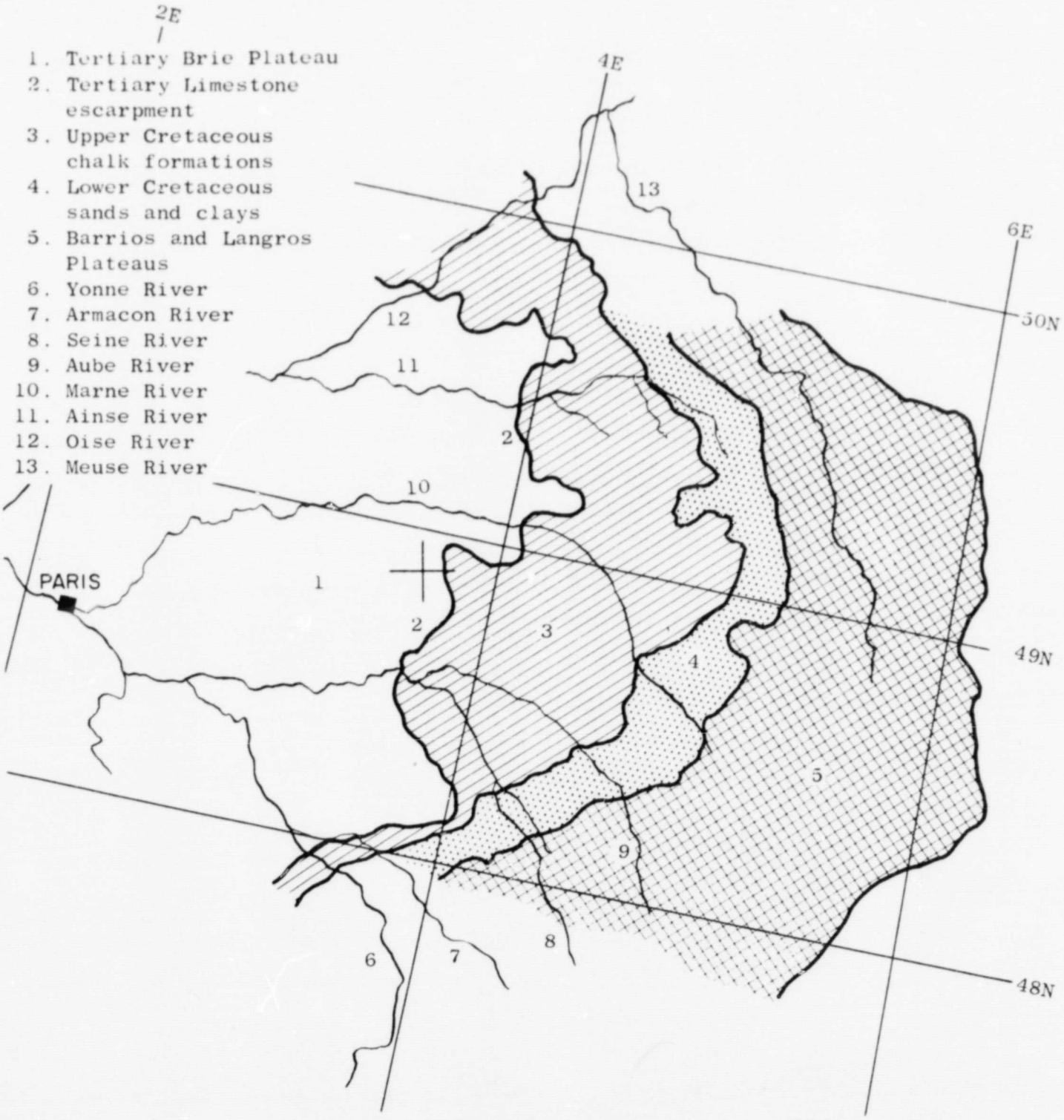

1. Tertiary Brie Plateau
2. Tertiary Limestone escarpment
3. Upper Cretaceous chalk formations
4. Lower Cretaceous sands and clays
5. Barrios and Langros Plateaus
6. Yonne River
7. Armacon River
8. Seine River
9. Aube River
10. Marne River
11. Ainse River
12. Oise River
13. Meuse River

Figure 2 General Structural Geology Map of Central France with Area Coverage Corresponding to Figure 1.

Although forest boundaries are known to mark geologic boundaries, it appears that forest cover alone cannot account for the very distinct and uninterrupted sizes and shapes of these tonal patterns. In these cases, it appears that the different reflectivities of the various rock-soil textures have a greater effect on tonal rendition than do the cultural/vegetation patterns which would normally be prominent on high altitude photography.

A question raised and a problem to be analyzed by these studies concerns where and under what conditions, various kinds of rock and soil types and textures can be identified and, concurrently, what types and under what conditions are vegetation and other patterns discernible from rock-soil types. Additionally, can changes in these parameters be detected with the passage of time.

In another case (Ref. 12) the tectonic map of the U.S.S.R. was revised through the use of a Nimbus I AVCS photograph (Fig. 3). What were considered to be several separate and independent fault zones in the Sayan Mountains (Pre-Baikal area) were revealed as one fault zone (East Sayan Fault) through analysis of a fresh snowfall pattern of the area. The difference in elevation on the two sides of the fault, with a corresponding difference in snow accumulation and reflectivity along the fault made it possible to infer the fault zone where it did not appear on maps. The fact that a few weeks earlier or later this pattern would have been obscured by lack of snow or too much of it reveals how unusual and unexpected may be the benefits from the analysis of these satellite photographs.

Close analysis of the U.S. Southwest in Nimbus photographs indicates that known tectonic and structural features of this area can be seen in these data (Ref. 13).

The Geological Survey has used Nimbus I AVCS to make the following significant cartographic changes in their 1:10,000,000 Antarctic plastic relief model (Ref. 14).

1. Mount Siple was repositioned 2^{o} west from the position given on existing maps. This is a 10,000-foot (3,000 meter) mountain, on the coast, often used as a location or orientation point.

2. A mountain group in the Kohler Range area was eliminated. (This group evidently was sighted by two different expeditions and subsequently positioned by them in two different locations. Antarctic maps currently show two mountain groups in this area, whereas Nimbus I photography indicates that there is only one group.)

3. The ice-front information was updated and the ice front itself reconfigured in the Filchner ice shelf, Weddell Sea, and Princess Martha Coast area (Fig. 4).

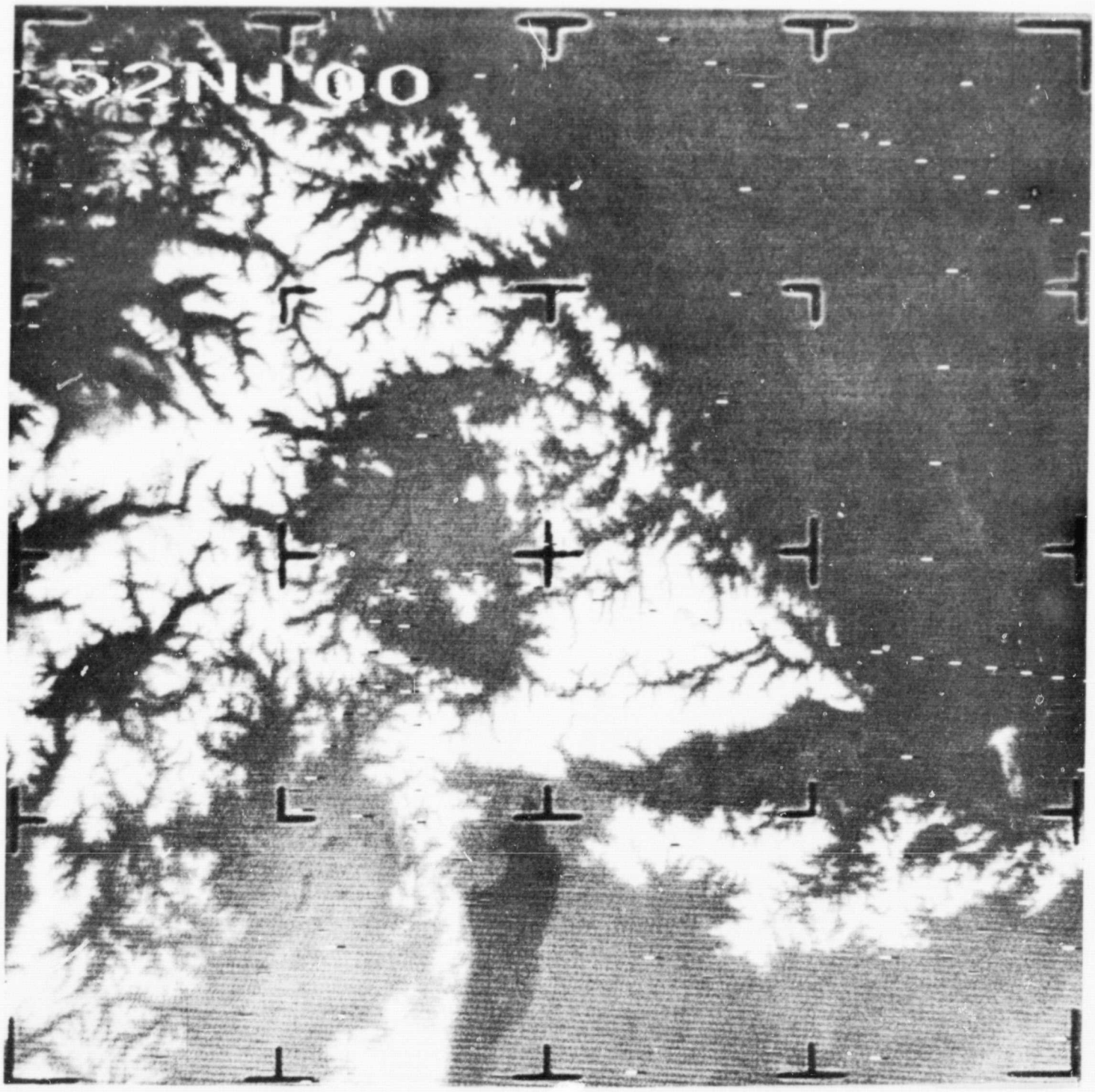

Figure 3 Nimbus I AVCS Picture of the Sayan Mountains, U.S.S.R. (Showing Fault Revealed by New Snow Pattern).

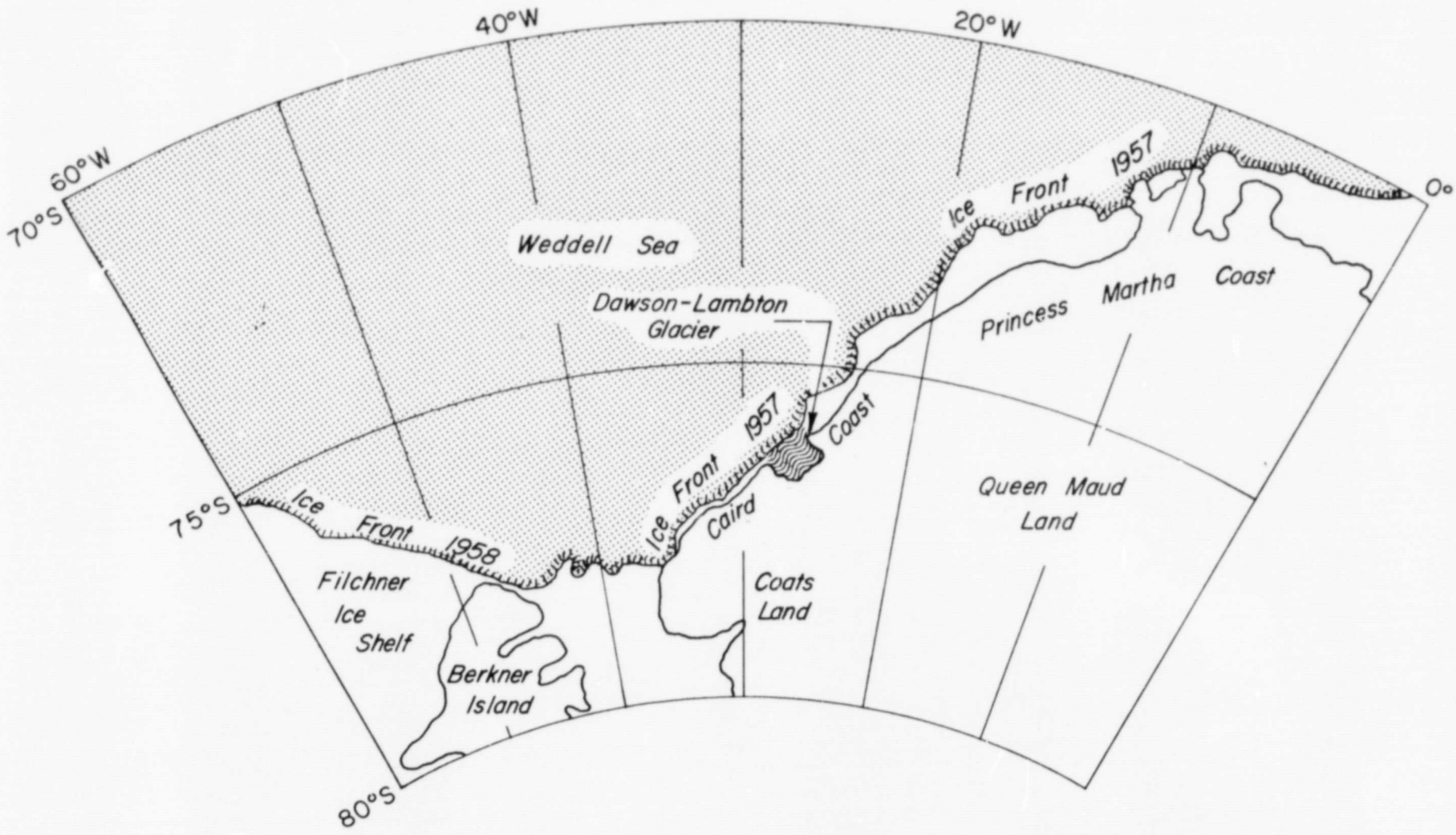

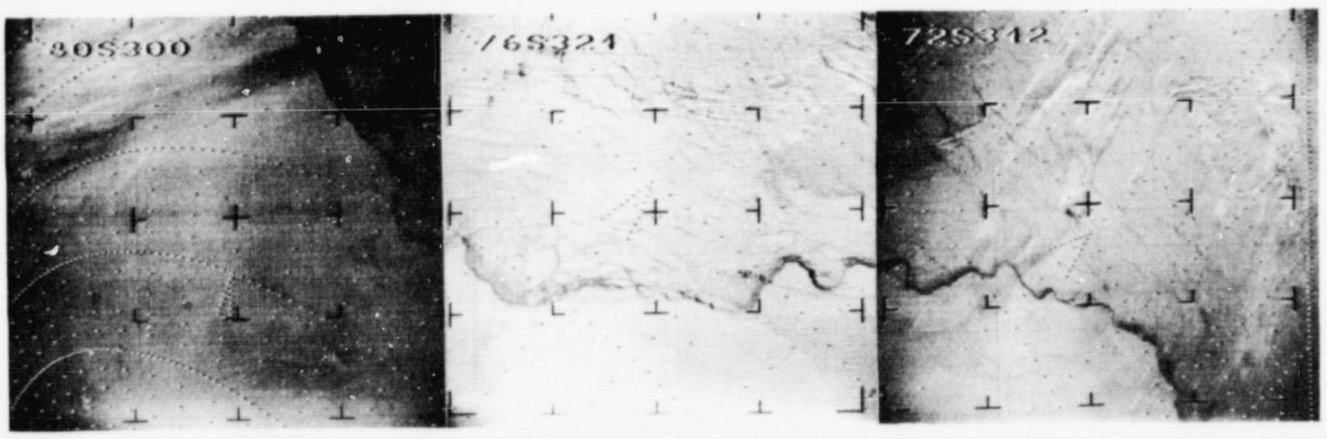

Figure 4 Nimbus I AVCS Picture of Antarctica with the Filchner Ice Shelf and Weddell Sea Prominent (Map after "Antarctica," Ref. 15).

Some AVCS photography has been used for sea ice studies. One case study of sea ice in the Foxe Basin of the Northwest Territory of Canada, using Nimbus I data, showed that the extent of sea ice as determined from the AVCS data was in very close agreement with sea ice observations reported by the Canadian Department of Transport for the same period (Ref. 16).

The Marine Division of the United Kingdom Meteorological Office has operationally used satellite APT data to supplement their conventional sources of sea ice information for their Arctic ice condition maps.

According to most experts in ice observing and forecasting, if photographs of Nimbus I quality could be obtained regularly, they could provide much of the sea ice information used in preparing long-range forecasts presently acquired through aerial ice reconnaissance.

In another study (Ref. 17), both the television and photofacsimile-constructed infrared pictures taken by Nimbus I were analyzed for indications of the pack ice boundary around Antarctica. Mean ice boundaries were established around the entire continent from both TV and infrared pictures, from which were estimated pack-ice areas of 19.81×10^6 and 16.78×10^6 square kilometers respectively.

Studies such as this, capable of being accomplished by Nimbus type data, will be needed for radiation and heat budget studies of the Antarctic and Arctic.

Nimbus II AVCS observations of ice floes along the east coast of Greenland for a month and a half were able to track an individual floe from Shannon Island to Kong Oscars Fjord, before it again merged with the coastal ice pack. These observations were then used to determine sea currents for that period in the area (Fig. 5). Ice amounts and limits, also, could have been mapped from these pictures.

In another case study Nimbus II tracked a 20 nautical mile long tabular iceberg in the Antarctic Ocean from the day after launch until the end of AVCS transmissions (Ref. 18 and Figs. 6 and 7 and Table 2). Apparent interaction between the iceberg and eddies in the Antarctic Convergence Zone revealed differences in current speed and direction (as could be expected) from the mean values given in an oceanographic atlas of the Antarctic (Ref. 19).

These last two case studies demonstrate the feasibility of using available satellite data for location, tracking and mapping of large scale ice phenomena, especially in remote areas.

Mapping snow cover amount and distribution, especially in flat non-forested terrain, appears to be an entirely feasible and practical application of satellite TV data (Refs. 20-23). In a study of the Missouri-Upper Mississippi River Basin snow

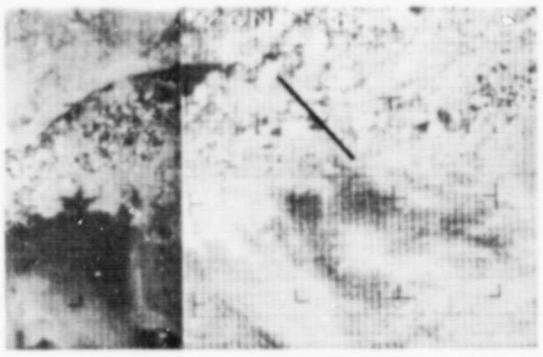

1 June 1966

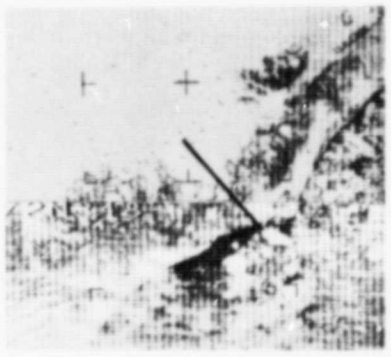

8 June 1966

21 June 1966

28 June 1966

5 July 1966

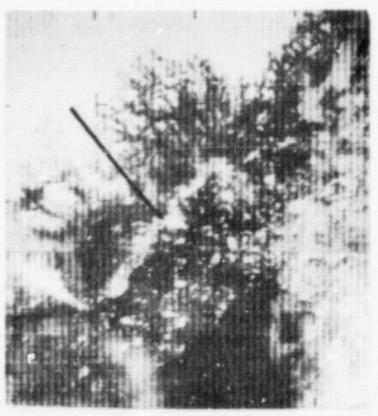

16 July 1966

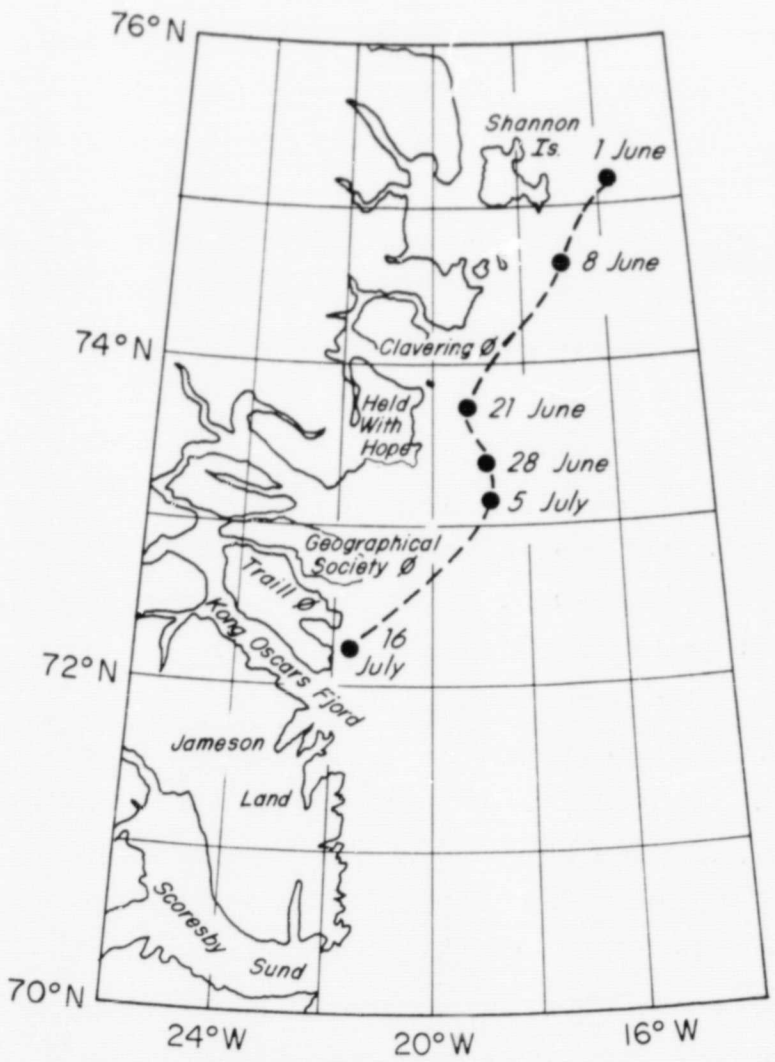

East Coast of Greenland from Shannon Island to Scoresby Sund

Figure 5 Nimbus II AVCS Observations of an Ice Floe Along the East Coast of Greenland.

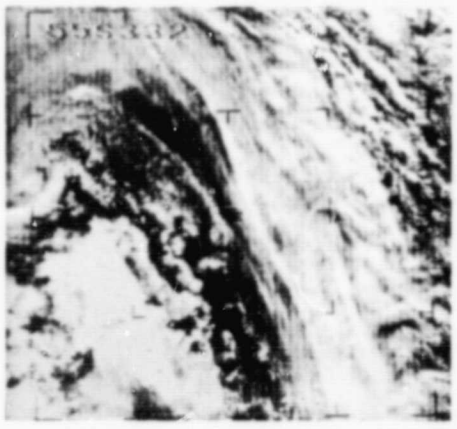

18 May 1966
Camera 3

30 May 1966
Camera 2

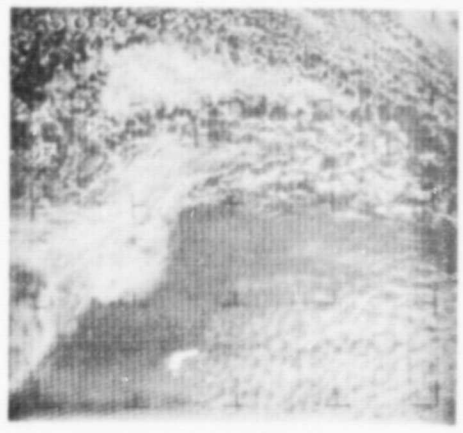

19 June 1966
Camera 2

23 June 1966
Camera 1

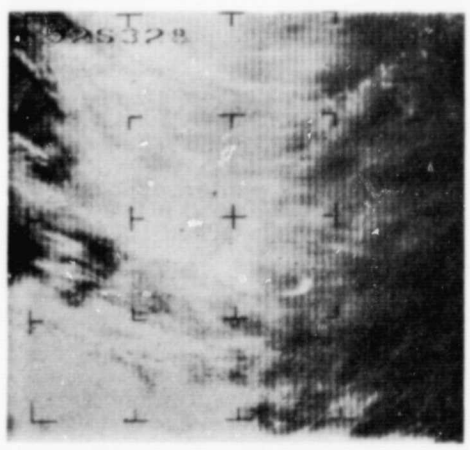

11 July 1966
Camera 2

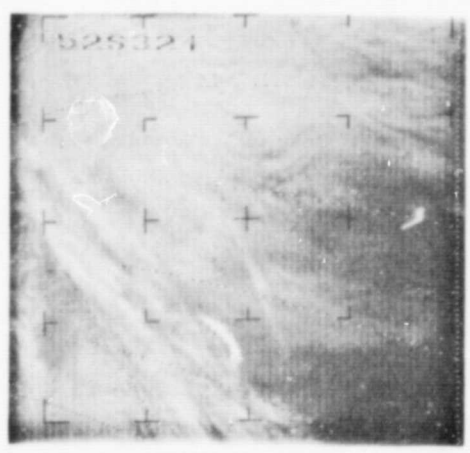

12 July 1966
Camera 1

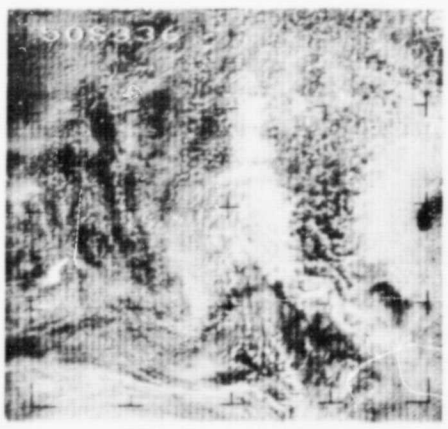

31 July 1966
Camera 2

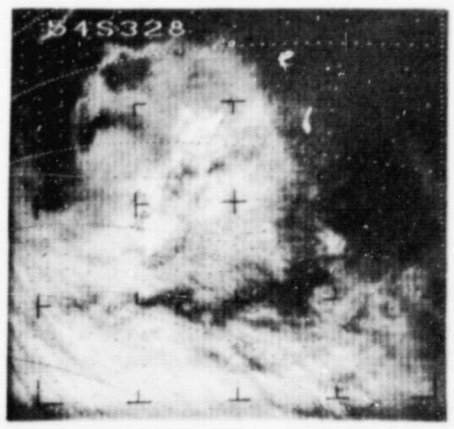

7 August 1966
Camera 1

20 August 1966
Camera 1

Figure 6 Nimbus II AVCS Pictures of an Antarctic Ocean Tabular Iceberg.

Table 2

Tabular Iceberg Locations for Selected Periods
From 18 May to 30 August, 1966

PERIOD	LATITUDE	LONGITUDE	OBSERVATIONS
18 May - 27 May	52.0S (12)*	31.0W (18)*	3
30 May - 20 June	52.3S (6)	28.7W (22)	8
23 June - 15 July	51.9S (18)	29.5W (29)	10
20 July - 31 July	51.4S (12)	29.0W (11)	4
2 Aug - 8 Aug	51.2S (18)	28.3W (18)	3
15 Aug - 17 Aug	52.4S (6)	25.8W (11)	2
20 Aug - 23 Aug	53.6S (18)	24.6W (22)	3
26 Aug - 30 Aug	53.6S (6)	22.8W (14)	2

*Maximum excursion in nautical miles from the average position.

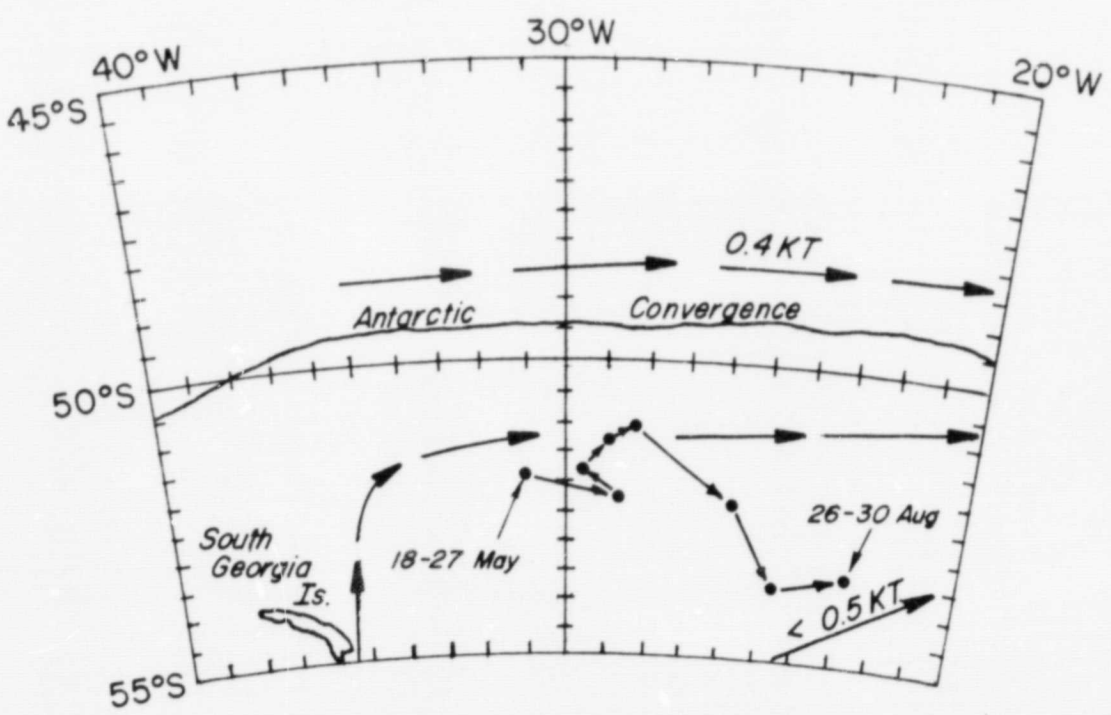

Figure 7 Conventional Current Directions and Speeds and Plotted Tabular Iceberg Locations for the Selected Periods Given in in Table 2. (Current Directions and Speeds and Convergence Zone Location are from Ref. 19.)

cover was mapped with TIROS and ESSA resolution satellite data with an accuracy of approximately ± 20 miles. One conclusion of the study was that satellite data can often provide a more detailed mapping of snow cover distribution than can be obtained through even the most complete conventional station network. Figure 8, a Nimbus II APT picture of the east coast of the United States, defines very well the area of recent snowfall.

A snow depth of one inch or more is detected by the satellite as a continuous snow cover. Snow depths of less than one inch are usually detected, but often do not appear as continuous cover. Areas with snow cover greater than about three inches in nearly all cases have reflectivities significantly higher than areas with lesser snow depths. The Nimbus II APT picture (Fig. 9) of the east coast of the United States shows a very bright Delaware-Maryland-Virginia peninsula blanketed the day before by an 8 inch snowfall. The rest of Maryland and Virginia received only a trace to 4 inches of snowfall and thus show lesser reflectivities.

Although it is obvious that present satellite photography cannot provide the quantitative measurements of snow depth provided by a network of surface stations, it can provide the limits of snow cover and detailed qualitative estimates of snow depth in the areas between reporting stations. This information is of much importance to hydrologists in making ground water runoff estimates and flood control forecasts.

The preceding studies document the fact that applications of satellite TV data to an earth resources program are entirely feasible even though they do not cover all of the possible applications of the data. Appropriate documentation materials could demonstrate the usefulness of the available Nimbus data for other earth resources applications and would indicate how improved sensor resolution and coverage would improve data extraction.

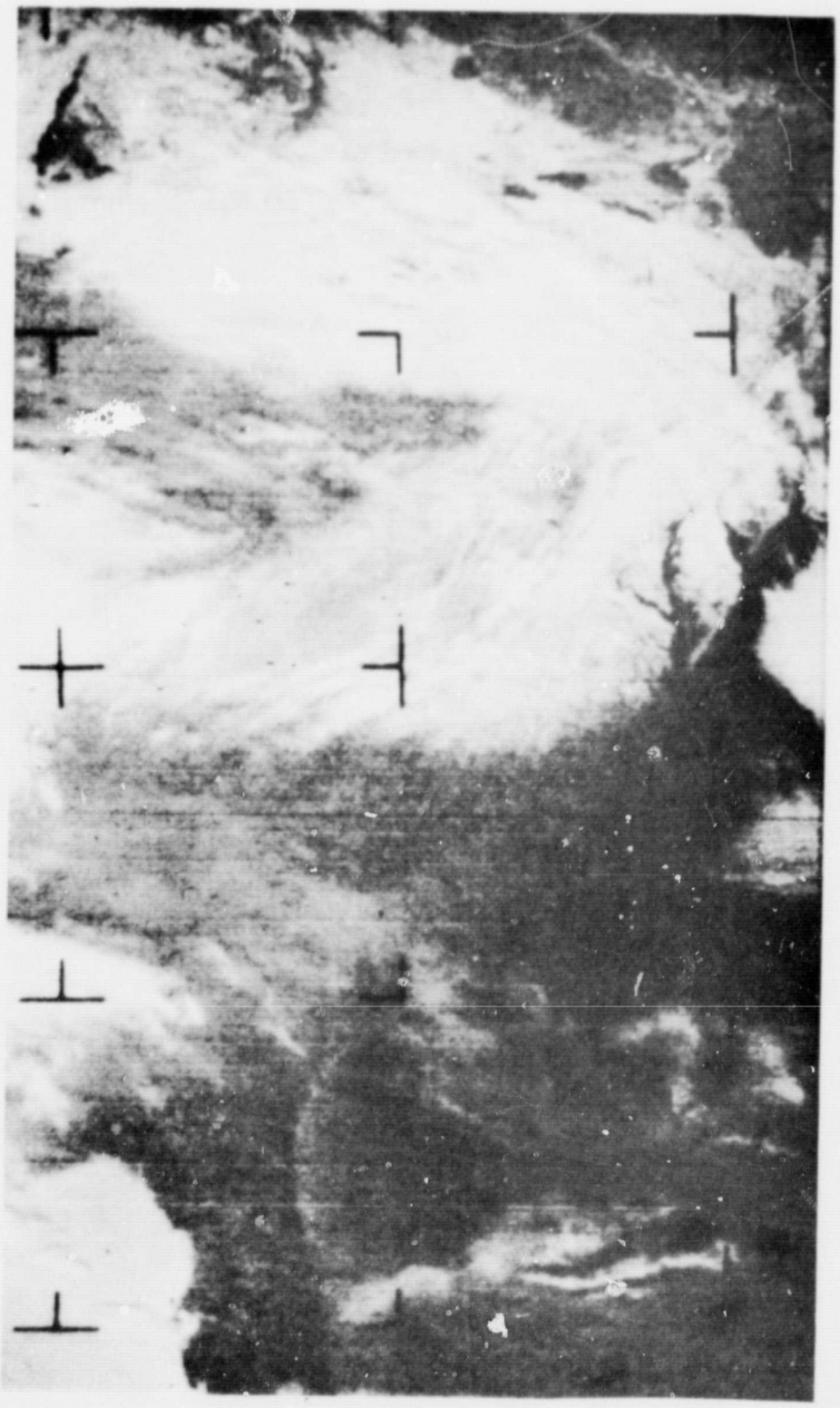

Figure 8 Nimbus II APT Picture from 27 December 1966 of the East Coast of the U. S. Defining the Area of Recent Snowfall.

Figure 9 Nimbus II APT Picture from 20 January 1967 Distinguishing Between a New Eight Inch Snowfall on the Del-Mar-Va Peninsula and Old Snow in Other Regions.

3. NON-METEOROLOGICAL APPLICATIONS OF NIMBUS RADIATION DATA

3.1 Introduction and Formats of Available HRIR Data

The HRIR system on Nimbus I and II provided equivalent blackbody temperatures of the earth surface and cloud tops by measuring the nocturnal radiation in the 3.5 to 4.1 micrometer (μm) atmospheric window. In the daytime, the radiation measured is a combination of reflected solar radiation and telluric radiation. Daytime data will be considered in Section 3.3.6. Coverage by the Nimbus I was limited by its short lifetime (August 28 - September 22, 1964) and its elliptic orbit which limited the readout time. Nimbus II HRIR had longer lifetime (May 15 - November 15, 1966) and in a nearly circular orbit, provided excellent world-wide coverage for an extended period of time. At a Nimbus height of 600 n.mi. the $1/2^{o}$ field of view of the sensor resulted in an instantaneous field of view of 5 n.mi. at the subsatellite point. On the spacecraft the radiometer scans the earth continuously at 44.7 RPM normal to the spacecraft direction. The instrument is designed to measure temperatures between 210K and 330K with a noise equivalent temperature difference of 1K for a background of 250K.

The HRIR data are available from the National Space Science Data Center (NSSDC) in the following forms:

1. A strip chart of the analog signal (Visicorder) as seen in Figure 10.
2. A photofacsimile strip build-up from the earth portion of successive scans (Fig. 11).
3. Nimbus Meteorological Radiation Digital Tapes (NMRT). The original analog data are digitized at a rate of 1000 samples per second, producing approximately 400 temperature values from horizon to horizon.
4. Temperature grid print maps, computer produced from the NMRT's (Figs. 14 and 16).
5. Computer listings of digitized temperature values with latitude-longitude values (Fig. 12).

The photofacsimile strips are valuable as a guide to the selection of cases for further study. The strip charts (visicorders) and computer listings are difficult to handle in any quantity. The temperature grid print maps are best suited for analysis. These grid print maps can be obtained from NSSDC in Polar Stereographic or

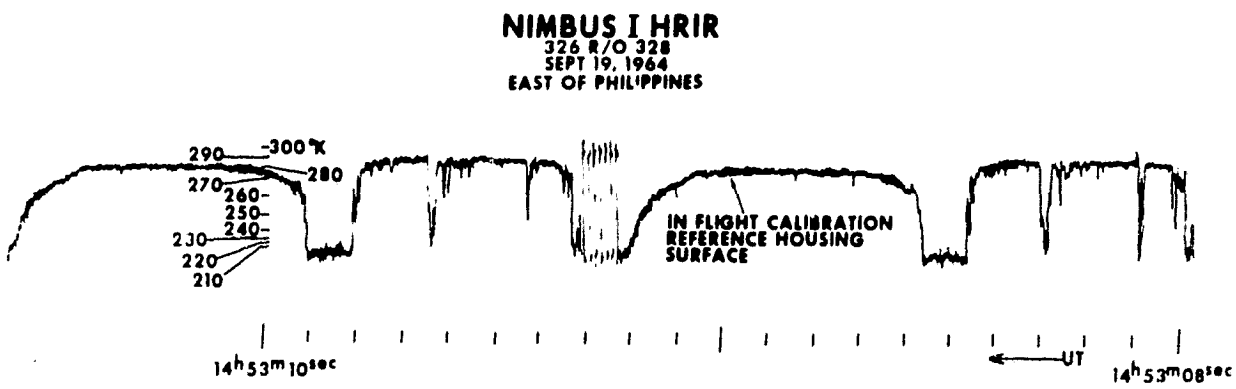

Figure 10 Portion of an Analog Record Showing Nearly Two HRIR Scan Cycles

Figure 11 HRIR Photofacsimile Showing the Eastern U.S. Area Observed at Night by the Nimbus II Satellite on 24 September 1966, Orbit 1756

NMRT-HRIR DATA FOR ORBIT1917 SWATH BEGINING AT 279 DAYS, 6 HOURS, 2 MIN. 53.8 SEC. PAGE 167
SUBSATELLITE LAT = 40.94 SUBSATELLITE LONG = 87.27

SPOT	NADIR	LATITUDE	LONGITUDE	HRIR-DATA	SPOT	NADIR	LATITUDE	LONGITUDE	HRIR-DATA
141	-19.851	41.749 N	92.306 W	277.3 I	193	-5.902	41.192 N	88.660 W	275.5
142	-19.582	41.739 N	92.228 W	277.3 I	194	-5.633	41.184 N	88.629 W	274.6
143	-19.314	41.728 N	92.150 W	274.6 I	195	-5.365	41.173 N	88.563 W	275.5
144	-19.046	41.718 N	92.073 W	273.7 I	196	-5.097	41.161 N	88.498 W	276.4
145	-18.778	41.707 N	91.996 W	273.7 I	197	-4.829	41.150 N	88.432 W	276.4
146	-18.509	41.697 N	91.919 W	275.5 I	198	-4.560	41.138 N	88.366 W	274.6
147	-18.241	41.686 N	91.843 W	277.3 I	199	-4.292	41.127 N	88.301 W	273.7
148	-17.973	41.676 N	91.768 W	278.1 I	200	-4.024	41.116 N	88.235 W	272.1
149	-17.705	41.665 N	91.692 W	278.9 I	201	-3.756	41.104 N	88.170 W	273.7
150	-17.436	41.655 N	91.618 W	278.9 I	202	-3.487	41.092 N	88.105 W	275.5
151	-17.168	41.644 N	91.543 W	278.1 I	203	-3.219	41.081 N	88.039 W	274.6
152	-16.900	41.634 N	91.469 W	276.4 I	204	-2.951	41.069 N	87.974 W	273.7
153	-16.632	41.628 N	91.443 W	273.7 I	205	-2.683	41.057 N	87.909 W	276.4
154	-16.363	41.617 N	91.369 W	272.9 I	206	-2.414	41.046 N	87.843 W	276.4
155	-16.095	41.607 N	91.296 W	278.1 I	207	-2.146	41.034 N	87.778 W	275.5
156	-15.827	41.596 N	91.224 W	282.4 I	208	-1.878	41.022 N	87.713 W	274.6
157	-15.559	41.586 N	91.151 W	282.4 I	209	-1.610	41.010 N	87.648 W	271.3
158	-15.290	41.575 N	91.078 W	278.9 I	210	-1.341	40.999 N	87.583 W	272.1
159	-15.022	41.565 N	91.006 W	274.6 I	211	-1.073	40.987 N	87.518 W	276.4
160	-14.754	41.554 N	90.934 W	274.6 I	212	-0.805	40.975 N	87.452 W	277.3
161	-14.486	41.543 N	90.862 W	277.3 I	213	-0.537	40.963 N	87.387 W	275.5
162	-14.217	41.533 N	90.790 W	278.1 I	214	-0.268	40.951 N	87.322 W	277.3
163	-13.949	41.522 N	90.719 W	273.7 I	215	0.0	40.939 N	87.258 W	277.3
164	-13.681	41.511 N	90.648 W	272.9 I	216	0.268	40.927 N	87.193 W	274.6
165	-13.413	41.501 N	90.576 W	277.3 I	217	0.537	40.915 N	87.128 W	273.7
166	-13.144	41.490 N	90.505 W	278.9 I	218	0.805	40.903 N	87.063 W	275.5
167	-12.876	41.479 N	90.435 W	277.3 I	219	1.073	40.890 N	86.998 W	276.4
168	-12.608	41.468 N	90.364 W	276.4 I	220	1.341	40.878 N	86.933 W	277.3
169	-12.340	41.458 N	90.294 W	275.5 I	221	1.610	40.866 N	86.869 W	278.1
170	-12.071	41.447 N	90.224 W	275.5 I	222	1.878	40.854 N	86.804 W	278.1
171	-11.803	41.436 N	90.154 W	276.4 I	223	2.146	40.842 N	86.739 W	277.3
172	-11.535	41.425 N	90.084 W	276.4 I	224	2.414	40.829 N	86.675 W	274.6
173	-11.267	41.414 N	90.014 W	277.3 I	225	2.683	40.817 N	86.610 W	273.7
174	-10.998	41.403 N	89.945 W	277.3 I	226	2.951	40.804 N	86.546 W	273.7
175	-10.730	41.392 N	89.875 W	277.3 I	227	3.219	40.792 N	86.481 W	275.5
176	-10.462	41.382 N	89.806 W	277.3 I	228	3.487	40.780 N	86.417 W	276.4
177	-10.194	41.371 N	89.737 W	277.3 I	229	3.756	40.767 N	86.352 W	276.4
178	-9.925	41.360 N	89.669 W	276.4 I	230	4.024	40.755 N	86.288 W	277.3
179	-9.657	41.349 N	89.600 W	276.4 I	231	4.292	40.742 N	86.223 W	278.9
180	-9.389	41.338 N	89.532 W	278.1 I	232	4.560	40.729 N	86.159 W	276.4
181	-9.121	41.327 N	89.464 W	279.7 I	233	4.829	40.717 N	86.095 W	272.9
182	-8.852	41.315 N	89.396 W	279.7 I	234	5.097	40.704 N	86.030 W	272.9
183	-8.584	41.304 N	89.328 W	276.4 I	235	5.365	40.692 N	85.966 W	276.4
184	-8.316	41.293 N	89.260 W	277.3 I	236	5.633	40.679 N	85.902 W	278.1
185	-8.048	41.282 N	89.193 W	278.9 I	237	5.902	40.675 N	85.880 W	278.9
186	-7.779	41.271 N	89.126 W	278.1 I	238	6.170	40.662 N	85.815 W	278.1
187	-7.511	41.260 N	89.059 W	277.3 I	239	6.438	40.649 N	85.751 W	275.5
188	-7.243	41.249 N	88.992 W	275.5 I	240	6.706	40.636 N	85.686 W	274.6
189	-6.975	41.237 N	88.925 W	273.7 I	241	6.975	40.623 N	85.622 W	276.4
190	-6.706	41.226 N	88.859 W	274.6 I	242	7.243	40.610 N	85.557 W	274.6
191	-6.438	41.215 N	88.792 W	277.3 I	243	7.511	40.597 N	85.492 W	273.7
192	-6.170	41.204 N	88.726 W	277.3 I	244	7.779	40.584 N	85.427 W	274.6

Figure 12 A Sample Computer Listing of HRIR Data.

Mercator projections at almost any scale. A 1:1,000,000 scale is appropriate for detailed temperature analysis. At this scale each temperature value on the grid print map is an average of 2 to 4 digitized temperature values, the number of values decreasing as the area mapped gets closer to the horizon.

3.2 Problems in the Analysis of HRIR Grid Print Temperature Maps

Before we can analyze a temperature map with any degree of confidence, we of course have to be aware of the problems with the data. Applications of the HRIR data to the Earth Resources Program are first of all limited by the resolution of the sensor (5 n.mi. at the Subsatellite Point). Nevertheless, procedures for solving HRIR data handling problems may be directly applicable to much higher resolution observations planned for Earth Resources Survey satellites.

3.2.1 Correction for Atmospheric Absorption

The equivalent blackbody temperatures mapped are not corrected for small atmospheric absorption in the 3.5 to 4.2 μm band caused by ozone, CO_2, and water vapor. Calculations by Kunde (Ref. 24) indicate corrections of about 1 to 2 K for a dry high-latitude atmosphere, and 2 to 5 K for a humid tropical atmosphere.

3.2.2 Assumption of Blackbody Emission

The assumption of blackbody emission also causes errors in the temperatures mapped. The temperatures mapped are obtained by means of Planck's law for a blackbody which relates the intensity of the radiation emitted I_{bb} by an object to its blackbody temperature, T_b. Thus,

$$dI_{bb} = \frac{C_1 \lambda^{-5}}{\exp \frac{C_2}{\lambda T_b} - 1} d\lambda \qquad (1)$$

where λ is wavelength, and C_1, C_2 are constants.

The intensity I_m measured by the Nimbus radiometer is

$$I_m = \int_{\lambda_1}^{\lambda_2} \phi(\lambda) \frac{C_1 \lambda^{-5}}{\exp \frac{C_2}{\lambda T_b} - 1} d\lambda = \int_{\lambda_1}^{\lambda_2} \phi(\lambda) B(\lambda, T_b) d\lambda \qquad (2)$$

where $B(\lambda, T_b)$ is the blackbody function and $\phi(\lambda)$ is the instrument's filter function over the wavelength interval $\lambda_1 - \lambda_2$, chosen to be 3.4 and 4.2μm respectively. The measured intensities I_m are used in the above equation to infer equivalent blackbody surface temperatures (T_b). Equation 2 applies only to blackbodies. Water surfaces and moist vegetated land radiate very nearly as blackbodies, but other earth surfaces depart somewhat from the blackbody assumption and radiate as gray bodies at a fraction, E, of their blackbody emission. Table 3 lists emissivities E of some common terrain features in the 3 to 5μm band (Ref. 25). Laboratory measurements by Hovis (Ref. 26), and Hovis and Callahan (Ref. 27) indicate that emissivities of many minerals in their natural state may be much less than unity. Thus, equation (2) becomes

$$I_m = \int_{\lambda_1}^{\lambda_2} E\phi(\lambda) B(\lambda, T_b) d\lambda \qquad (3)$$

where E is the emissivity of the surface. An average emissivity $\bar{E}$ can be defined for the spectral interval λ_1 to λ_2 and

$$I_m = \bar{E} \int_{\lambda_1}^{\lambda_2} \phi(\lambda) B(\lambda, T_b) d\lambda \qquad (4)$$

It is therefore clear that the emissivity of a surface affects the derived temperature map. Except for water surfaces and moist vegetated land with emissivities nearly equal to one, the temperatures mapped are lower than the actual surface temperatures. Figure 13 gives the relationship between the measured intensities I_m and the equivalent surface temperatures for E = 1 (Ref. 28) and E = 0.9 for the Nimbus II radiometer. Temperatures on the maps are plotted

Table 3

Emissivity of Common Terrain Features in the 3-5μm Range*

Green Mountain Laurel	E = 0.90
Young Willow Leaf (dry, top)	0.94
Holly Leaf (dry, top)	0.90
Holly Leaf (dry, bottom)	0.86
Pressed Dormant Maple Leaf (dry, top)	0.87
Green Leaf Winter Color - Oak Leaf (dry, top)	0.90
Green Coniferous Twigs (Jack Pine)	0.96
Grass - Meadow Fescue (dry)	0.82
Sand - Hainamanu Silt Loam - Hawaii	0.84
Sand - Barnes Fine Silt Loam - S. Dakota	0.78
Sand - Gooah Fine Silt Loam - Oregon	0.80
Sand - Vereinging - Africa	0.82
Sand - Maury Silt Loam - Tennessee	0.74
Sand - Dublin Clay Loam - California	0.88
Sand - Pullman Loam - New Mexico	0.78
Sand - Grady Silt Loam - Georgia	0.85
Sand - Colts Neck Loam - New Jersey	0.90
Sand - Mesita Negra	0.75
Bark - Northern Red Oak	0.90
Bark - Northern American Jack Pine	0.88
Bark - Colorado Spruce	0.87

* (from Ref. 25)

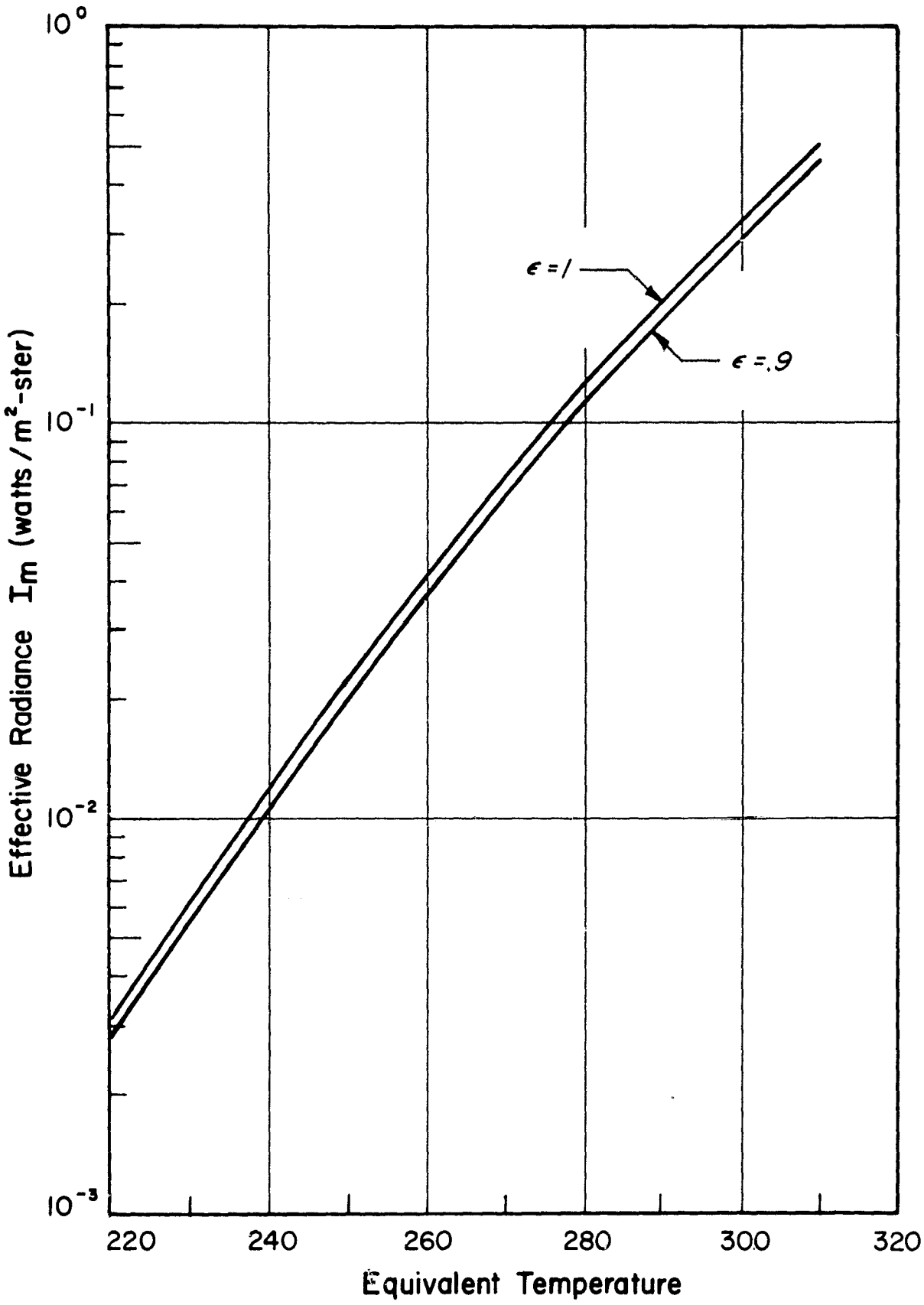

Figure 13 Relationship Between Effective Radiance, I_m, Measured by the Nimbus II HRIR and Equivalent Surface Temperature, for an Emissivity of 1 and 0.9.

assuming an emissivity E, equal to one and therefore are somewhat in error. For example, an emissivity of 0.9 would cause a surface temperature of 290 K to be plotted as 288 K. The greatest errors, of the order of 2 to 4 K would occur over sandy regions of relatively low emissivities.

3.2.3 Errors in the Relative Location of Successive Scans

Another problem with the digitized HRIR temperature maps is the error that the mapping computer makes in the relative location of successive scans. The computer positions the scan by locating the horizons and placing the subsatellite point midway between the horizons. An error in the location of the horizons can therefore cause an error in the scan position. Assuming that the computer routine is in error by one digitized sample in locating the horizon then the error expressed in angular measurements is

$$e = \frac{360 \ \frac{\text{degrees}}{\text{revol.}}}{1000 \ \frac{\text{samples}}{\text{sec.}} \ 1.342 \ \frac{\text{sec.}}{\text{revol.}}} \approx 0.3 \ \frac{\text{degrees}}{\text{sample}}$$

which corresponds to about 3 n. mi. positioning error at the subsatellite point and greater toward the horizons. The computer routine that locates the subsatellite point can be in error by more than one digitized sample, since it involves the location of both horizons each of which can be in error by one or more samples. These location errors are most evident at temperature discontinuities outlining coastlines normal or nearly normal to the scan. The meanders (of the order of 5 to 10 n. mi.) in the apparent position of the coastline of Lake Michigan in Figure 14 are thought to be caused by this mapping error. A more refined determination of the horizons in the mapping program is thus necessary to improve the relative scan-to-scan location accuracy of the data. The absolute location accuracy of the data is of course affected mostly by excursions of the satellite attitude from zero (assumed in the mapping) and by uncertainties in the satellite ephemeris data. Nevertheless, the absolute location can be refined by reference to known landmarks such as coastlines, rivers, etc.

Some investigators at the Goddard Laboratory for Atmospheric and Biological Sciences, Environmental Science Services Administration, and at the Naval Oceanographic Office have been successful in building a "rectified" grid print map from the

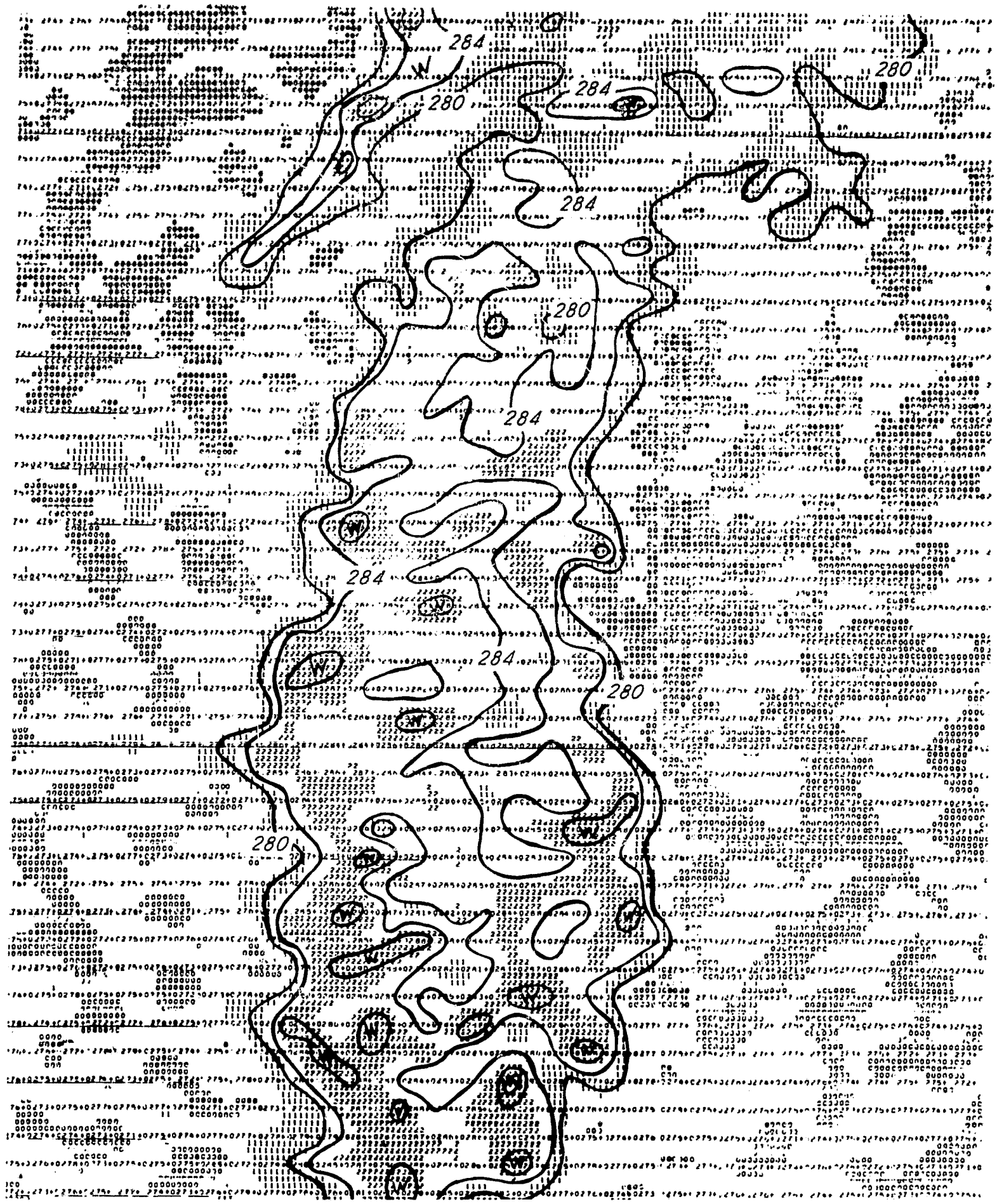

Figure 14 Digitized HRIR Temperature Map of Lake Michigan Produced by NSSDC. Temperatures are in Degrees Kelvin. Scale of Original is 1:1,000,000. Isotherms are Drawn Only for the Lake Area from 280K at 4K intervals. Data are Unfiltered. Area was Observed by Nimbus II at Night on 6 October 1966, Orbit 1916. The Warmest Lake Areas are Labeled by a W.

computer listings of the digitized temperature values (Fig. 12). Each scan is collated on a base map in the position best fitting known landmarks such as a coastline. This type of analysis is time consuming and only applicable to small areas near the sub-satellite point.

3.2.4 Noise

A spectrum analysis (Fig. 15) performed by ARA personnel on Nimbus II HRIR analog data revealed noise that peaked at 200 Hertz. This noise limited accuracy of Nimbus II HRIR by causing errors of as much as 3K. The Nimbus I HRIR is noisier than the Nimbus II HRIR as revealed by visual inspection, and by a spectrum analysis performed by J. Kennedy at LABS (Ref. 29). The Nimbus I HRIR has periodic noise at 16 Hertz, and oscillatory noise at 100, 200, 300 and 400 Hertz (Ref. 58). The 16 Hertz noise shows up on the photofacsimile as diagonal lines. It is therefore best to work with the "cleaner" and more abundant Nimbus II HRIR.

A spectrum analysis such as was done on the Nimbus data will aid in pinpointing any noise. Once the characteristics of the noise are determined, possible causes can be sought, and ways to eliminate it can be devised, if the noise originates during the ground processing of the data. If the noise originates on the satellite, as was the case in the Nimbus I and II HRIR, the final digitized temperature data can still be passed through a numerical filter which will attenuate this noise. A computer program that produces filtered HRIR temperature maps has been developed by ARA personnel and is now in use at the Goddard Laboratory for Atmospheric and Biological Sciences (LABS) although data obtained through NSSDC are not filtered. Figure 16 is the filtered version of the Lake Michigan area shown in Figure 14.

3.2.5 ARA Digital Color Printer for the HRIR

A machine for displaying HRIR temperature maps in color has been developed by ARA. A subroutine (provided by ARA) on the HRIR mapping program at LABS causes the temperatures to be encoded on standard computer cards. The cards are then passed through the ARA Digital Color Printer which translates the encoded temperatures into predetermined colors on a photographic plate. A color can be made to represent a temperature or temperature interval. Colors can be selected

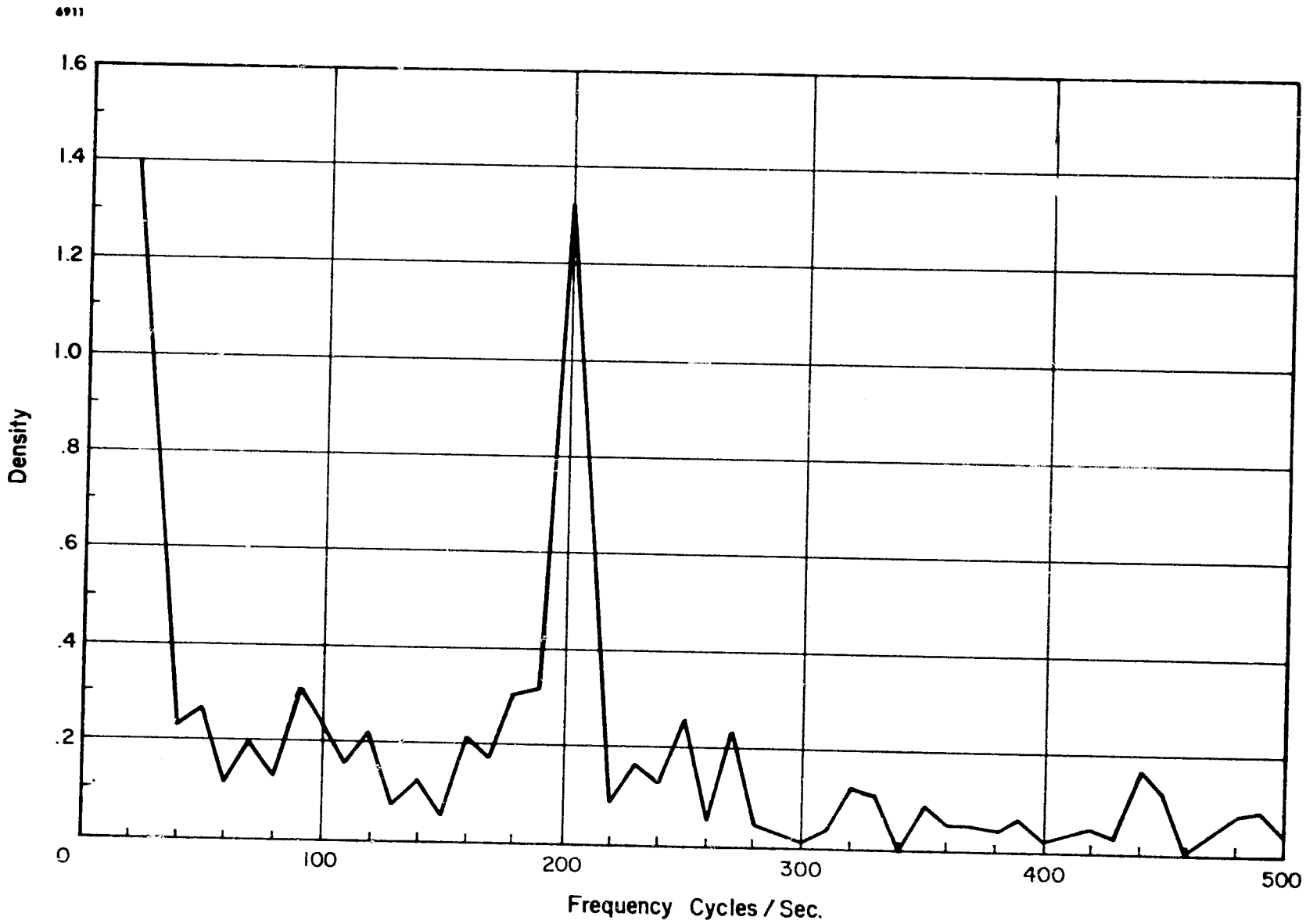

Figure 15 Spectrum Analysis Performed on a Nimbus II HRIR Analog (Visicorder) Scan. The Relatively Uniform Backscan Portion was Used for the Analysis.

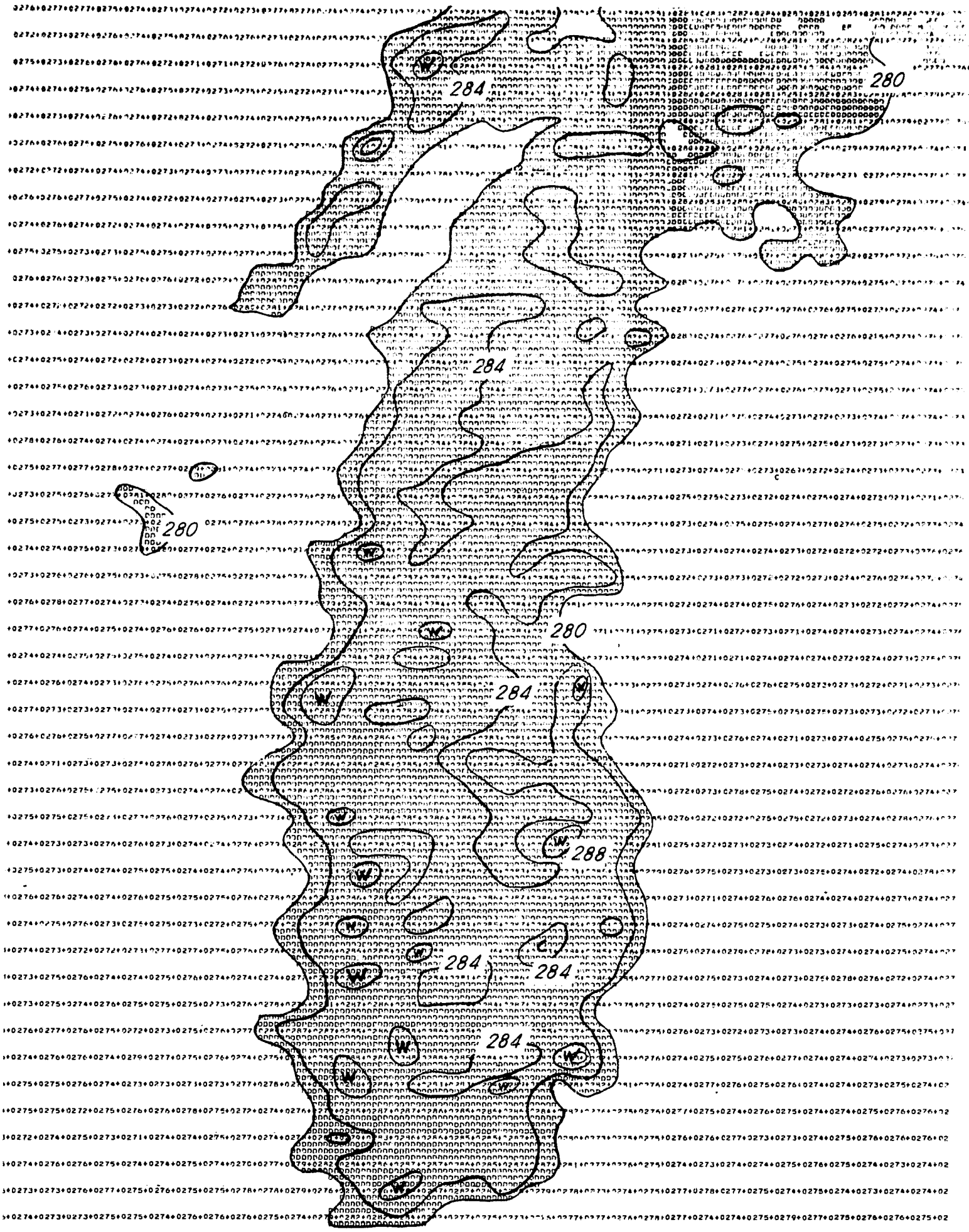

Figure 16 Filtered Version of Digitized HRIR Map of Lake Michigan Shown in Figure 14.

to enhance contrast between certain ranges of temperatures thus facilitating analysis. Figure 17 shows a sample color print version of an HRIR temperature map of the Gulf Stream area (Ref. 30). The data were recorded at local midnight on 28 August 1966 during pass 1396 of Nimbus II. Each colored square is about 7.5 miles. Each of the nine colors represents a 2 degree Kelvin temperature increment ranging from 300K at the red end to 283K and cooler in the blue.

3.3 Factors Influencing Surface Temperatures and Their Variation

The problems with the HRIR data outlined above are not unsurmountable, and the temperature maps as presently available from NSSDC (no filtering, no correction for scan-to-scan location error) can and have been utilized for relatively fine analyses applicable to earth resources problems.

Nimbus measurements of infrared radiation provide spatial temperatures at a given time of night over a few months space. The problem is to relate the spatial temperature differences and the long term march of temperature over an area to properties of the surface and subsurface.

For a water surface the temperature per se is a most important parameter directly related to currents, the productivity of the waters and, in some cases, define fishing grounds. Mapping of water surface temperatures and their significance will be covered in Section 3.4. We shall briefly discuss the factors that influence surface temperature and their variation.

3.3.1 Elevation

The temperature pattern in the HRIR data faithfully reproduces the elevation of the ground features, according to the altimetric rule of 5 to 10K decrease per kilometer of higher elevation (5K/km for wet adiabatic, 10K/km for day adiabatic circulation). One is therefore interested in detecting temperature deviations from the altimetric rule caused by differing properties of the surface and subsurface.

Figure 17 Digital Color Printer Output (Nimbus II, Pass 1396)

7064

3.3.2 Heat Budget of the Earth's Surface

The earth surface gains or loses energy and therefore varies in temperature by:

1. Direct and scattered solar radiation from the sky (E_o). A fraction of this short-wave energy is reflected from the surface and thus unavailable to heat the surface.

2. Infrared radiation emitted through the atmosphere and lost to the atmosphere (R_o) proportional to the surface emissivity and to the fourth power of the surface temperature.

3. Sensible flux of heat in the atmosphere (L_o), usually by turbulent transfer of a mass of air (convection).

4. Sensible flux of heat within the soil (B_o), due to molecular conduction or the complex heat transfer process occurring in moist soils. B_o is related to the thermal conductivity (λ) of the soil, and influenced by the subsurface heat capacity (c), and the vertical gradient of soil temperature.

5. Latent heat of phase transformation (evaporation or condensation of water), W_o.

The losses and gains of energy by these processes constitute the heat budget at the surface and may be expressed as

$$E_o + R_o + B_o + L_o + W_o = \Delta Q_o \qquad (5)$$

ΔQ_o represents the net gain or loss of energy over a given period of time of a very thin layer just at the surface and is therefore related to the changes of surface temperatures. ΔQ_o is zero over a long period of time. A quantitative evaluation of the terms in Equation (5) is extremely complex and only possible under idealized conditions since it requires an a priori knowledge of surface and atmospheric conditions. Assume for the sake of investigating the various terms in Equation (5) that we have a surface temperature field at sea level or at a uniform height. Further, assume the sensible flux of heat (L_o) and the latent heat of transformation (W_o) constant over the area under observation. Under these assumptions spatial differences of temperature are to be attributed to spatial differences in those properties of the surface influencing E_o, R_o, and B_o.

3.3.2.1 Surface Properties Influencing the Absorption of Solar Radiation, E_o

E_o, the relative amount of solar radiation absorbed by the surface, is controlled by the surface albedo (assuming that the area is small enough to eliminate latitudinal variations). Dark areas (low albedo) absorb more, light areas (high albedo) less. Figure 18 shows the results of an analysis by Estoque and Yee, (Ref. 31) of the surface temperature as a function of albedo for given initial conditions. The black surface shows much higher temperatures and higher diurnal temperature amplitudes than the white surface. A land surface of high albedo is expected to show lower temperatures at night than a surface of low albedo under similar conditions.

3.3.2.2 Surface Properties Influencing R_o, The Energy Lost by the Surface by Infrared Radiation

R_o, the energy lost by the surface by infrared radiation over all wavelengths is proportional to the emissivity of the surface, the turbidity of the atmosphere (its gaseous and particulate contents), and the fourth power of the temperature. If the turbidity and temperature of the atmosphere may be assumed the same over the area under consideration, variations of R_o are caused by variations in surface temperatures, and surface emissivities only. Under similar conditions warm and highly emissive surfaces will lose energy and therefore cool faster than cold low emissive surfaces.

3.3.2.3 Surface Properties Influencing B_o, the Sensible Flux of Heat

B_o, the sensible flux of heat near the surface is controlled by the thermal properties of the surface and subsurface. A natural parameter which expressed the thermal properties of substances composing the earth's surface is $(\rho\, c\, \lambda)^{1/2}$ appropriately called the thermal property, with ρ, c, λ as the density, specific heat, and thermal conductivity of the substance. The thermal property depends on the condition and composition of the soil, on its structure and, most important, on

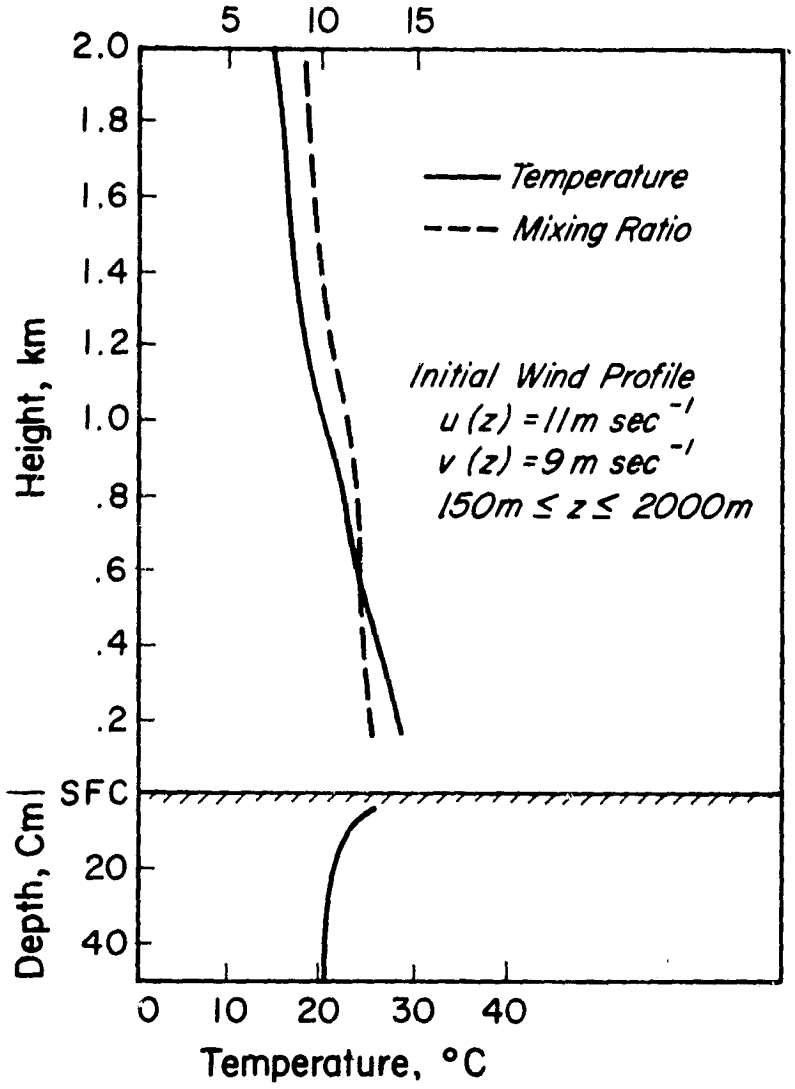

a. Initial Conditions

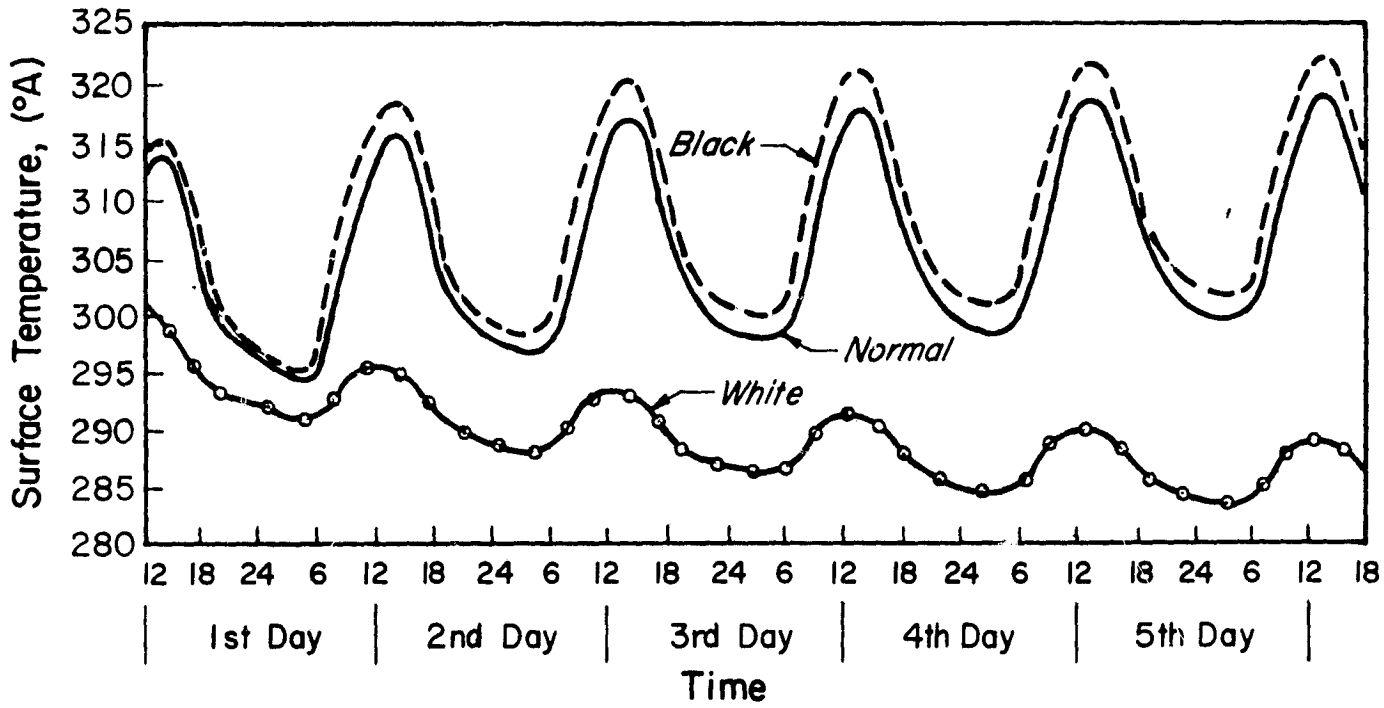

b. The Evolution of the Surface Temperature as a Function of Albedo

6069

Figure 18 Results of an Analysis by Estoque and Yee (Ref. 31).

its moisture content. Table 4 lists the density, specific heat, thermal conductivity, and thermal property for some typical ground types. The thermal property of the surface has a substantial control on the fluxes of heat between the ground and the air. If the thermal property is large, the subsurface absorbs a great amount of heat during the day and then conducts a great amount of heat to the radiating ground surface during the night. Temperature variations of the surface and the air layer near the surface are consequently moderate. Ground of poor thermal property conducts little heat to the subsurface, and accordingly the surface transmits much heat to the air during the day and receives little heat from the subsurface at night. Thus, the surface attains high temperatures in the daytime and low temperatures at night.

3.3.2.4 The Heat Budget of a Desert Surface

An extremely simplified situation is approximately met over calm desert regions at night, where the shortwave radiation (E_o), the sensible flux of heat in the atmosphere (L_o), and the latent heat of transformation (W_o) are zero or negligible, and the sensible flux of heat in the soil, B_o, is balanced by R_o, the radiation lost by the surface. Thus

$$B_o = \lambda \left(\frac{\partial T}{\partial z}\right)_o = R_o \tag{6}$$

where z is depth in the soil, T is temperature, and λ is the thermal conductivity. By a consideration of the heat conduction equation, Brunt (Ref. 32) has analyzed this situation in predicting the nighttime fall of surface temperature after sunset. He obtained the following equation for the nighttime march of surface temperature:

$$T_o(t) = T_{oo} - \frac{2 R_{oo}}{(\rho c \lambda)^{1/2}} \left(\frac{t}{\pi}\right)^{1/2} \tag{7}$$

where t = time after sunset and the subscript oo refers to the time $t = 0$ (sunset) and surface $z = 0$. Equation 7 shows that for given initial conditions, the greater the drop in temperature with time the smaller the value of $(\rho c \lambda)^{1/2}$, the thermal property of the soil. At a particular time of night under similar atmospheric conditions the surface temperature would be lower over surfaces with low values of the

Table 4

Thermal Conductivity λ, Specific Heat c, Density ρ, and Thermal Property $(\lambda c \rho)^{1/2}$ for Various Surfaces

SURFACE	λ	c	ρ	$(\lambda c \rho)^{1/2}$
	(cal/deg cm sec)	cal/deg g	g/cm^3	$cal/(cm^2 deg\ sec^{1/2})$
Concrete	0.0058	0.22	2.47	0.0566
Sandy Clay (15% moisture)	0.0022	0.33	1.78	0.0359
Pasture Clayland	0.0067	$c\rho = 0.56$		0.0199
Quartz Sand (dry)	0.00063	0.19	1.65	0.014
Still Water	0.0015	1.000	1.000	0.04
Turbulent Water (ocean)	1 to 100	1.000	1.000	1 to 10

thermal property than over surfaces with high values of the thermal property. A synoptic surface temperature map of a flat desert region would therefore, represent relative values of the thermal property. Thus, spatial measurements or gradients of surface temperatures can be employed to differentiate between surfaces of different thermal property.

3.3.3 Terrain Features Detectable By Synoptic Surface Temperature Patterns

Moisture has the greatest effect on the temperature field of a relatively flat area (Refs. 33, 34, 35, 36, and 37). Moisture-laden terrain cools less rapidly than dry areas, therefore, appears warmer in the nighttime temperatures. Drainage basins can thus be delineated (Refs. 33 and 38). The delineation of drainage basins is most important to guide the search for new water supplies. In semi-arid areas temperatures can map those areas that can store more humidity and therefore requiring a minimum of irrigation for agricultural activities (Ref. 33). Superficial and subterranean structural features such as faults, fractures, joints, and lineations can all be located by temperature patterns as shown by HRIR observations over North Africa and the Southwest U.S. analyzed by Pouquet (Refs. 33 and 34), and Pouquet and Raschke (Ref. 35). The reason is mainly that humidity, or ground water has a tendency to accumulate along these geological formations (Refs. 33, 34 and 35). It is possible, because of differences in the thermal property, for infrared imagery to show contact zones between different types of material as well as contact zones in similar material of different geologic age (Ref. 39). Thus, through an improvement of surface geology, infrared temperature maps can aid in delineating specific areas of interest for further mineral exploration so that efforts can be concentrated on detailed examination of those localities having a high success potential (Ref. 38).

Effects of albedo differences on nocturnal temperature patterns are presented in References 33, 34, 35, 36 and 37. Nordberg and Samuelson (Ref. 36) and Nordberg (Ref. 37) have examined the Salar de Atacama area in Chile. An anomalous warm ring around the Salar was attributed to deposits of dark volcanic material absorbing more solar radiation than the highly reflective Salar. Pouquet (Refs. 33 and 34) and Pouquet and Raschke (Ref. 35) examined areas of North Africa and found that nighttime measurements are closely related to solar reflectances over the same area. The absence of this expected relationship frequently helps in the detection of other geomorphical features such as rock formation and soil moisture.

Presence of volcanic activity may also be detected by the infrared temperatures. Surtsey, a new volcanic island 20 miles off the southwest coast of Iceland was observed as a very hot spot on the Nimbus II HRIR. Surtsey first appeared above the sea on November 14, 1963 (Refs. 40 and 41). Figure 19 is a Nimbus II HRIR photofacsimile observation of Surtsey on September 8, 1964. The warm island and ocean area show up as a dark spot (indicated by arrow). Figure 20 is a visicorder trace of four scans through the same area. The island at this date was only two square kilometers, nevertheless, the high temperatures of the ocean and land made it quite discernible in the middle two scans as a sharp spike.

3.3.4 Terrain Features Possibly Detectable by Temporal Surface Temperature Changes

3.3.4.1 Lettau's Approach to the Heat Budget Equation

A more complex approach to the heat budget equation was attempted by Lettau (Ref. 42). He analyzed the heat budget equation of the earth's surface with all its terms included, and showed that it is possible to explain surface temperature oscillations in terms of external conditions and the physical properties of the soil and atmosphere. The theory is, of course, the simplest and best applicable to places on the earth where these external conditions are relatively constant and well defined, such as desert regions. From Lettau's theory it is possible to relate the times of diurnal and annual maximum temperatures of different surfaces to the thermal property $(\rho \lambda c)^{1/2}$. Lettau's theory shows that for given atmospheric conditions, ground types having a large value of the thermal property have relatively small diurnal and annual amplitudes of surface temperatures, and have the temperature maxima occurring later in the day and in the year. For example, over the ocean with a thermal property larger than land, the temperature maximum occurs later in the day and year than over land, and annual amplitudes are smaller than over land. Figure 21 constructed from results given by Lettau (Ref. 42) relates the diurnal and annual time of maximum temperature with the thermal property.

Lenschow and Dutton (Ref. 43) measured surface temperature variations from an airborne radiometer over several surface types. They found that the diurnal variation is greatest over flat farmland and sandy field areas. Hilly woods and fields showed the smallest diurnal variation. The full exploitation of diurnal temperature variations for surface identification will have to wait the advent of a high resolution day-night radiometer (in the 10μm band) planned for future Nimbus flights.

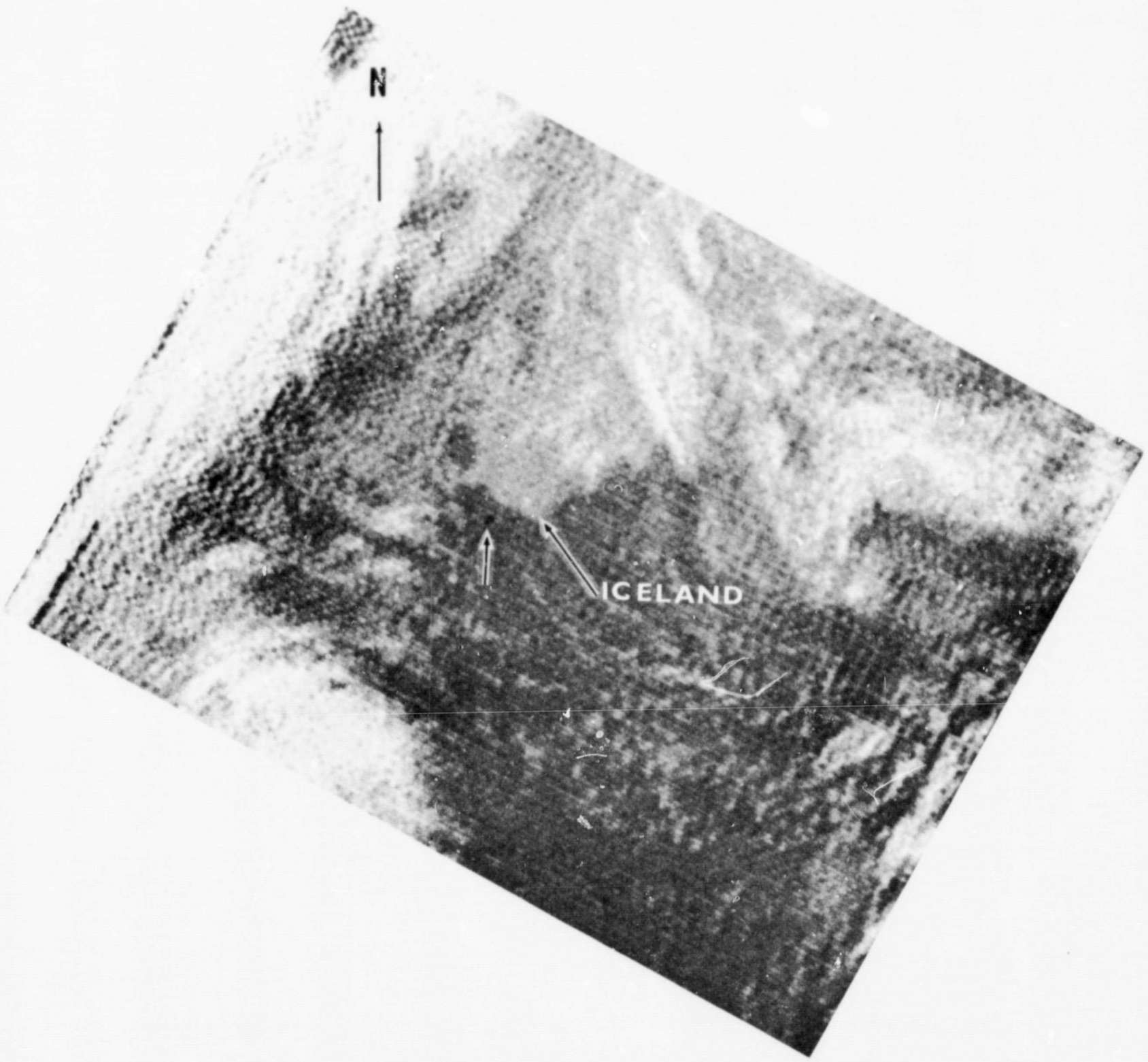

Figure 19 Nimbus II HRIR Photofacsimile Observation of Surtsey on 8 September 1966, Orbit 1541. The Surtsey Area Shows Up as a Dark Spot (Indicated by Arrow) off the Southwestern Coast of Iceland.

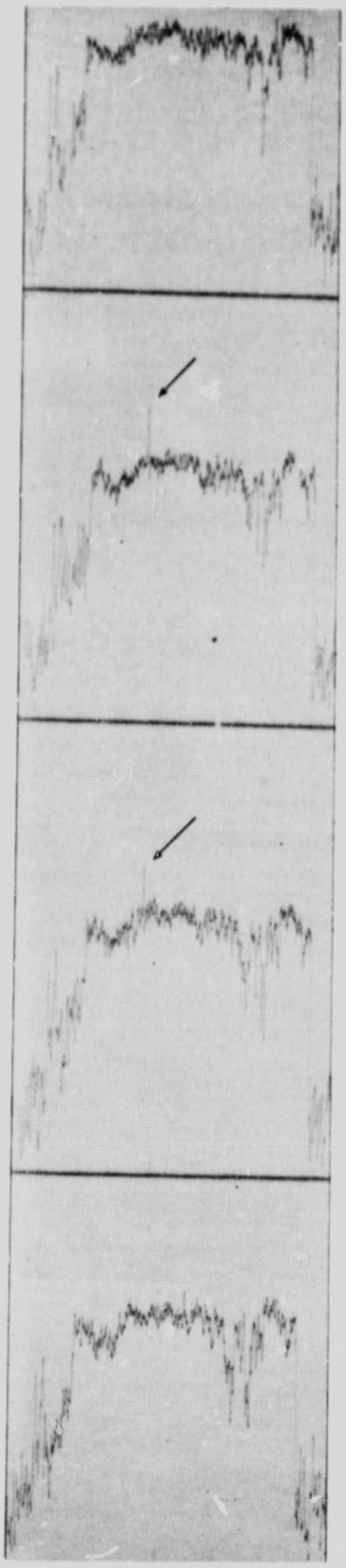

Figure 20 Four Scans of the Nimbus II HRIR Through the Surtsey Area on 8 September 1966. Surtsey Shows Up as a Spike in the Middle Two Scans.

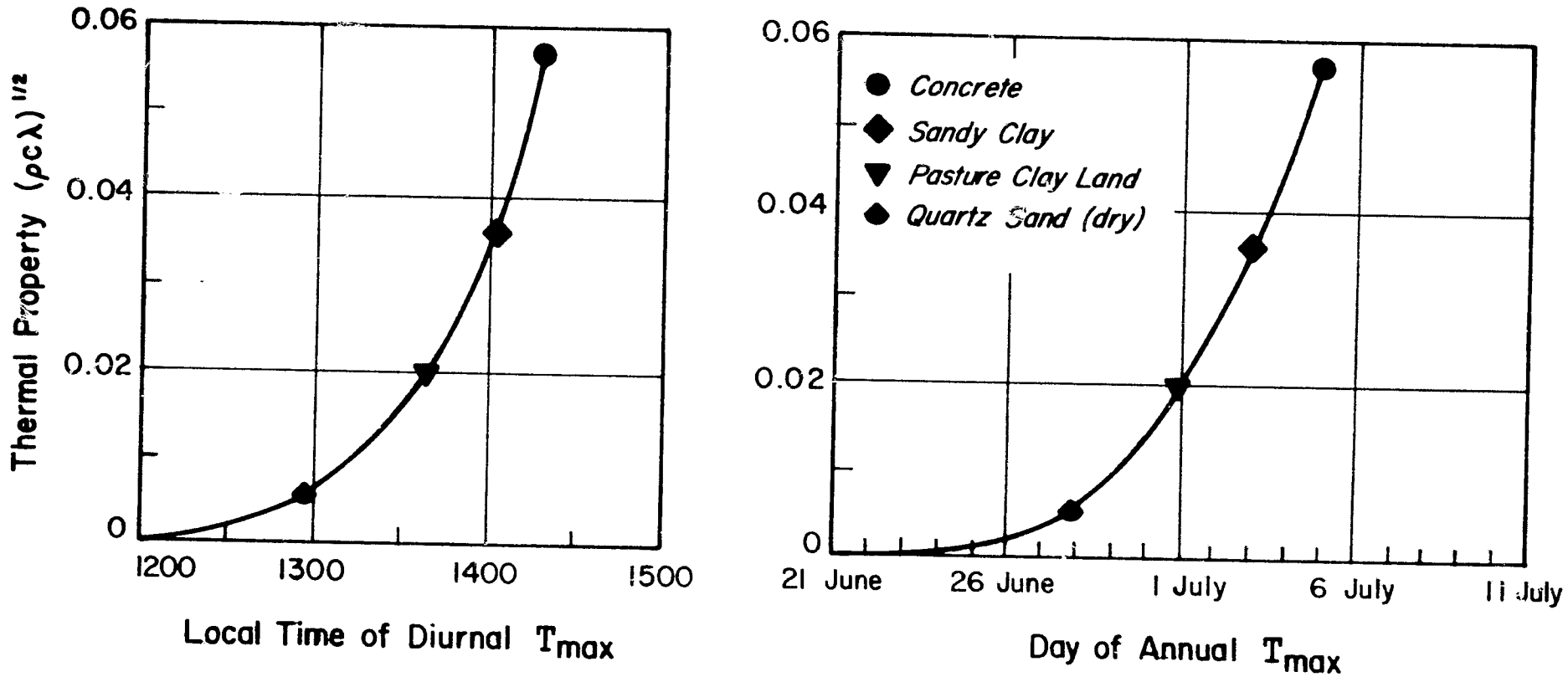

Figure 21 Diurnal and Annual Time of Maximum Temperature as a Function of the Thermal Property $(\rho c \lambda)^{1/2}$. Constructed from Data Furnished by Lettau (Ref. 42).

3.3.4.2 The Concepts of an "Equivalent Thermal Property" and a "Time Temperature Signature"

Nimbus HRIR temperature measurements do not permit us to follow the diurnal temperature cycle, since observations over any particular place are made only once a night. Nevertheless, it is possible to plot the seasonal trend of temperatures for any particular place during the lifetime of Nimbus II (May 15 - November 15, 1966). Curves similar to that for Lake Michigan presented in Figure 22 could be plotted from Nimbus HRIR data for various small areas of the earth. This kind of analysis is best feasible over desert regions where data are most plentiful because of least cloudiness and where Lettau's theory can be applied. The amplitude and the time of annual maximum temperature obtained from a best fit curve to the data could be used to estimate an "equivalent thermal property" for the area. The temperature versus time curve itself is related to the make-up of the surface and subsurface and would be the "time-temperature signature" for a particular area. Thus, with the aid of Nimbus II HRIR temperatures, an initial catalog of "time-temperature signatures" and "equivalent thermal properties" can be compiled for various well-known desert surfaces of the earth. Such a catalog would be useful in classifying poorly known regions of the earth. In instances where the signature does not correspond to the expected for that type of surface, other causes are to be suspected. Ground moisture would influence the shape of the curve because it would increase its thermal property. If the differences cannot be explained by presence of ground water a re-evaluation of surface or subterranean geology may be in order. Thus the "time-temperature signature" could be a means to detect comparative abundance and possible changes in ground moisture over a long period of time, and a reason to review and possibly revise the geology of an area. It is also feasible and useful to catalog "signatures" for various known types of vegetation cover. When the surface observed by the HRIR is vegetated the temperature measured is that of the top of the vegetation cover. Even though the low albedo of a vegetation cover tends to favor large variations of temperature at its outer boundary, its inhomogeneity and the air trapped within creates a thick absorption layer preventing the occurrence of very high temperatures in the daytime. The same characteristics favor low temperatures at its outer boundary during the night, but this is not the same temperature that would exist in the absence of vegetation.

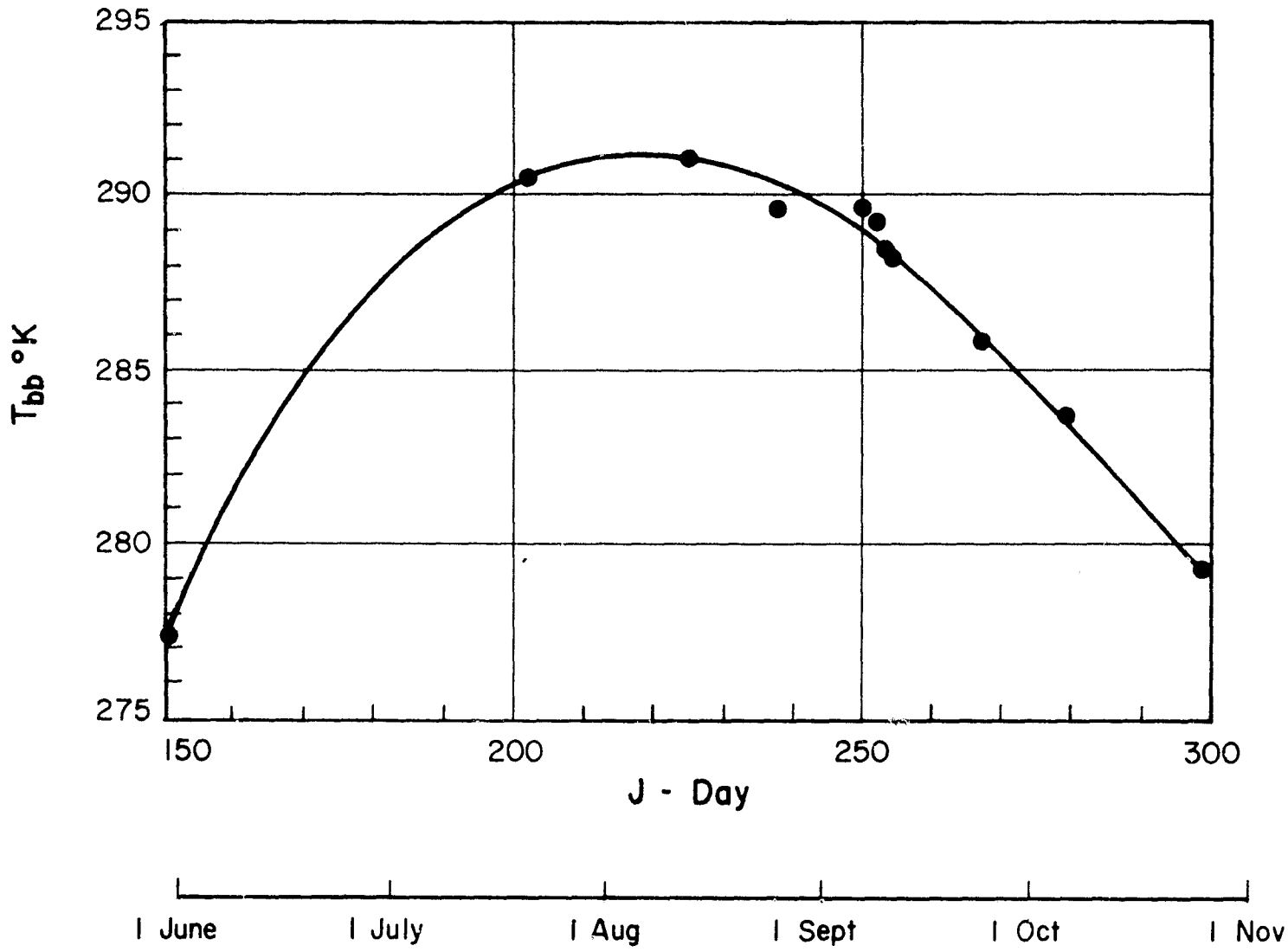

Figure 22 Average Surface Temperature Progression for Lake Michigan Obtained from Nimbus II HRIR Digitized Maps, June-October 1966.

It is doubtful whether different types of vegetation can be distinguished by "time-temperature signatures," nevertheless, it is hoped that the signature would be at least indicative of the thickness and changes in thickness of vegetation cover, and would distinguish between cultivated and bare land.

At present the six months of Nimbus II HRIR available could be used to construct partial time-temperature signatures for selected small areas of the earth to test the concepts outlined above and establish the methodology of investigations. The partial curves from the Nimbus data would show for the Northern Hemisphere the time of annual maximum temperature, and possibly the relative amplitude of the annual temperature wave.

In the future when earth resources satellites will provide continuous data year after year, yearly comparison of signatures of a locality may indicate long time changes in the vegetation, ground moisture; whether an area, for example, has been deforested, turned over to cultivation or pasture, or left uncultivated. Of course, year to year changes in climate for a particular area would cause a change in the shape of its signature. It is expected that the change would be mainly in the amplitude of the curve. Thus, to discriminate between the effects on the curve of a change in climate and a change in surface properties, it may be necessary to make nearby area comparisons, together with year to year comparison of the same area.

The method of signature comparison would depend greatly on correct location of the data. This is not too difficult at present with Nimbus HRIR maps. Temperature maps can be correctly relocated by known features such as coastlines, lakes, etc.

The amount of data available for a certain place depends on its cloud climatology. A desert region may be observed almost every night, while a region in middle latitudes will have fewer observations. This explains the few observations of Lake Michigan in Figure 22. Nevertheless, it was possible to draw a reasonably representative time-temperature signature curve for Lake Michigan. Sherr, Glaser and others (Ref. 44) prepared probability distributions for world-wide cloud coverage based on Nimbus data. Their report provides statistical information enabling one to determine the number of orbital passes needed to photograph or see any particular surface area on the earth.

3.3.5 Daytime HRIR Measurements

A few Nimbus I and II HRIR measurements were taken in the daytime. Daytime measurements do not reveal true surface temperatures because there is an appreciable contribution by reflected solar radiation in the 3.4 to 4.2μm band of the radiometer. Nimbus I daytime measurements are not applicable to quantitative analyses since they are highly contaminated by spurious shortwave radiation entering the radiometer. The most probable cause of the malfunctioning was considered to be an uncoated rim or crack of the interference filter (Ref. 45). The following analysis applies therefore only to the Nimbus II daytime measurements.

The measured daytime radiation I_m is approximately

$$I_m = \bar{r} \int_{3.4}^{4.2} S(\lambda)\, \phi\,(\lambda)\, d\lambda + \bar{E} \int_{3.4}^{4.2} B(\lambda, T)\, \phi\,(\lambda)\, d\lambda \qquad (8)$$

where $S(\lambda)$ is spectral radiance due to reflected solar radiation in the direction of the satellite. S can be computed solely from geometrical considerations from that portion of the solar constant falling between 3.4 and 4.2μm.

$B(\lambda, T)$	is spectral radiance due to thermal emission (Planck's function)
$\phi\,(\lambda)$	is effective spectral response of the instrument
$\bar{r}$	is reflectivity or albedo of surface averaged over the 3.2 to 4.2μm band
$\bar{E}$	is emissivity of the surface averaged over the 3.4 to 4.2μm band
$\bar{E}$ and $\bar{r}$	are related by Kirchhoff's law which states that $E = 1 - \bar{r}$

Equation (8) does not consider atmospheric scattering or absorption, which could be included as correction factors to $S(\lambda)$ and $B(\lambda, T)$. Equation (8) can be integrated to give:

$$I_m = (1 - \bar{E})\, I_s + \bar{E}\, I_{bb} \qquad (9)$$

where I_s and I_{bb} are that portion of the solar and terrestrial radiation sensed by the radiometer. For solar radiation at nearly vertical incidence I_s is of the order of

1 Watt/m^2 - ster. Maps of daytime HRIR data show values of equivalent blackbody temperatures T, corresponding to the radiation I_m measured by the radiometer. These are not the surface temperatures for the reasons explained above.

The right side of Equation (9) contains two unknowns, the surface temperature (implicit in the Planck's function) and the emissivity. Daytime data cannot give adequate surface temperatures without an assumption of E. Nevertheless for surfaces of uniform emissivity such as oceans, daytime radiation patterns (expressed in T_{bb} on maps) should faithfully reproduce temperature patterns.

Even ocean areas may exhibit different emissivities due to different states of the water surface, and different look angles. Observations of the Gulf Stream boundaries in the daytime HRIR (Fig. 23) may therefore be emphasized also by a change in sea state besides the temperature gradients. Presence of fog, however tenuous, would change the emissivity of the area observed and therefore affect the daytime radiation measurements. Fog, or low clouds in many instances are a locator of the Gulf Stream.

Cursory analyses of daytime data in desert regions suggest that the radiation patterns per se are related to the surface make-up but the contribution of emissivity and temperature cannot be separated.

Using I_s as 1 Watt/m^2 - ster in Equation (9), a graph of I_m versus equivalent temperature for various emissivities was constructed (Fig. 24). Mapped temperatures are calculated assuming an emissivity of 1. The graph shows the overwhelming effect of emissivity which totally masks low temperatures unless emissivities are very high, nearly 1. Even at high temperatures above 280K the solar radiation contribution is of the same magnitude as the telluric radiation for emissivities of 0.9 or less. Daytime measurements would serve therefore as qualitative indicators of land surfaces of low emissivities. When the surface temperature is known, accurate measurements of surface emissivities can be made (Ref. 36).

Global mapping of emissivities is of primary geologic interest, since these would be related to surface mineral deposits. Nimbus II daytime data would be useful in establishing relationships between the laboratory measurements of emissivities of various minerals and soils and orbital measurements of emissivities of the same minerals in their natural state and blended with impurities (Ref. 36).

At low temperatures emissivities can be estimated without a knowledge of the temperature (Ref. 36) since, for example, below 270K and E = 0.9, the telluric radiation is one order of magnitude or less than the solar reflected radiation. This suggests that daytime HRIR measurements could be used to map emissivities over

Figure 23 Nimbus II Daytime HRIR Photofacsimile Showing the Gulf Stream Boundary and the U. S. East Coast Area on 24 June 1966, Orbit 537.

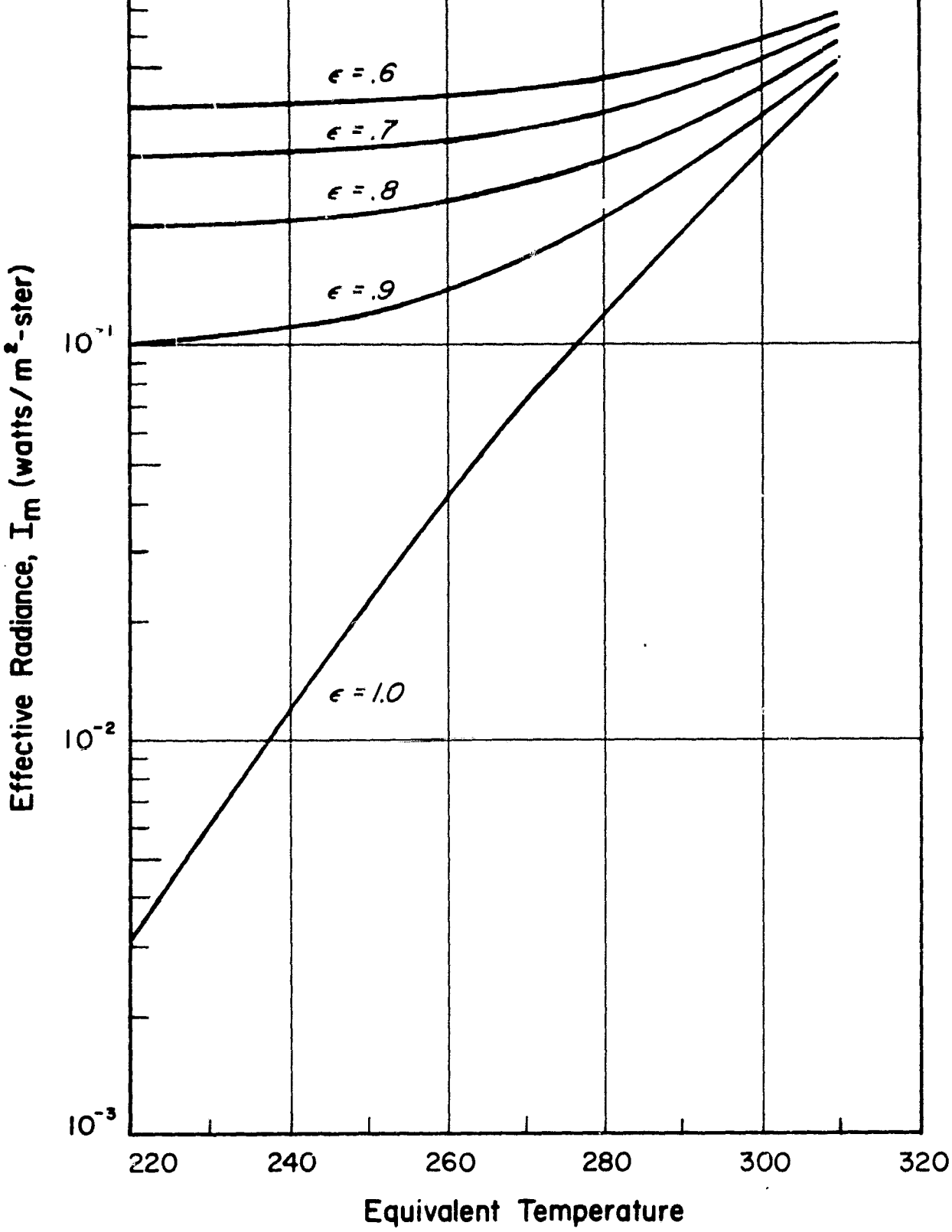

Figure 24 Daytime Effective Radiance I_m, Measured by the Nimbus II HRIR and Equivalent Surface Temperature for Various Surface Emissivities. The Solar Radiation Detected by the Radiometer at Normal Incidence and 100% Reflectivity (zero emissivity) is Assumed to be 1 watt/m^2-Steradian, in the Calculations.

mountainous regions without having to worry about orographic effects on temperatures. The satellite observations, by detecting relative surface emissivities, may be useful in narrowing down areas for further mineral exploration in those parts of the world, such as the Andes and Himalayas, which are thought to be rich in mineral deposits.

3.4 Temperatures of Water Surfaces

3.4.1 Sea Surface Temperatures

The need for repetitive measurement of the sea surface temperature for large areas of the world's oceans is becoming increasingly important. Nearly all of man's sea-oriented activities such as fisheries, navigation, and marine weather forecasting rely to some extent upon knowledge of the temperature patterns and their variation with time. Satellite borne instruments can provide the needed information on these temperature gradients and, with the application of proper ground truth information for calibration, will provide absolute temperature values.

Forecasts of fish availability for certain species rely in part on predicted changes in ocean temperature. Often, preferred fishing areas occur at the confluence of oceanic currents or at thin boundaries. In areas of upwelling such as those off the western coasts of most large land masses, nutrient-rich waters are brought to the surface, providing an excellent feeding ground for the larger fish. All of these phenomena can be detected through the measurement of sea surface temperature, which can in turn lead to the discovery of new fishing areas, or to a far more efficient use of existing fishing facilities.

Various investigations have demonstrated direct correlations between the sea surface temperature and such meteorological phenomena as the growth and travel of hurricanes, and extratropical cyclonic development. The probabilities of icing or of fog formation can also be determined. Recently there has been renewed interest in the field of long-range weather forecasting which takes into account the very significant role played by the oceans in determining the world-wide weather patterns.

A complete bibliography on the uses of satellites for oceanographic observations has been published by Widger and Greaves (Ref. 46). Reference 30 presents observations of ocean surface temperatures made by Nimbus II HRIR in the Gulf Stream area (Fig. 17).

3.4.2 Surface Temperatures of Lakes

Detection of lake surface temperature variations may help in identifying zones of different biological activity. Successive maps of surface temperature will yield information on currents. Information on lake currents will help establish the general circulation of lakes, and thus aid in the understanding of lake dynamics and estimating probable future distribution of pollutants added to lakes. Seasonal changes in temperature regulate the amount of distribution and kind of fish in a lake. Figure 25 (from Ref. 47) is a rendition of a digitized map of the Lake Erie areas. The increased eutrophication of Lake Erie is of great concern; temperature maps such as this will help establish circulation patterns and identify areas of thermal pollution.

3.5 Energy Budget Calculations

The five channel MRIR radiometer flown on Nimbus II is best suited to calculate the radiation terms in the energy budget of large areas. Raschke and Pasternak (Ref. 48) used the MRIR shortwave reflectance channel (0.2 to 4.0μm) and the thermal radiation channel (5.0 to 30.0μm) to compile the global radiation balance for the period 1 to 15 June 1966, Raschke, Moller, and Bandeen (Ref. 49) compiled the radiation balance over the polar region from Nimbus II MRIR measurements. Pasternak (Ref. 50) compiled an atlas of total outgoing long-wave radiation and of shortwave reflectances from Nimbus II MRIR observations. Energy budget calculations for given areas are useful in the improvement of agricultural planning and irrigation needs.

3.6 Mapping of Snow and Ice

The HRIR can complement the AVCS system with nighttime observations of snow cover extent and can measure the surface temperature of the snow cover, a significant parameter for predicting snow melt (Ref. 51).

Snow covered surfaces reflect a large amount of the incident solar irradiance during daytime hours and hence do not warm as much as relatively adjacent snowless surfaces. Therefore, snow covered surfaces will presumably be colder than non-snow covered surfaces, and so can be detected in the HRIR at night.

Snow pack determination is important in assessing water resources for summer irrigation and hydro-electric power generation.

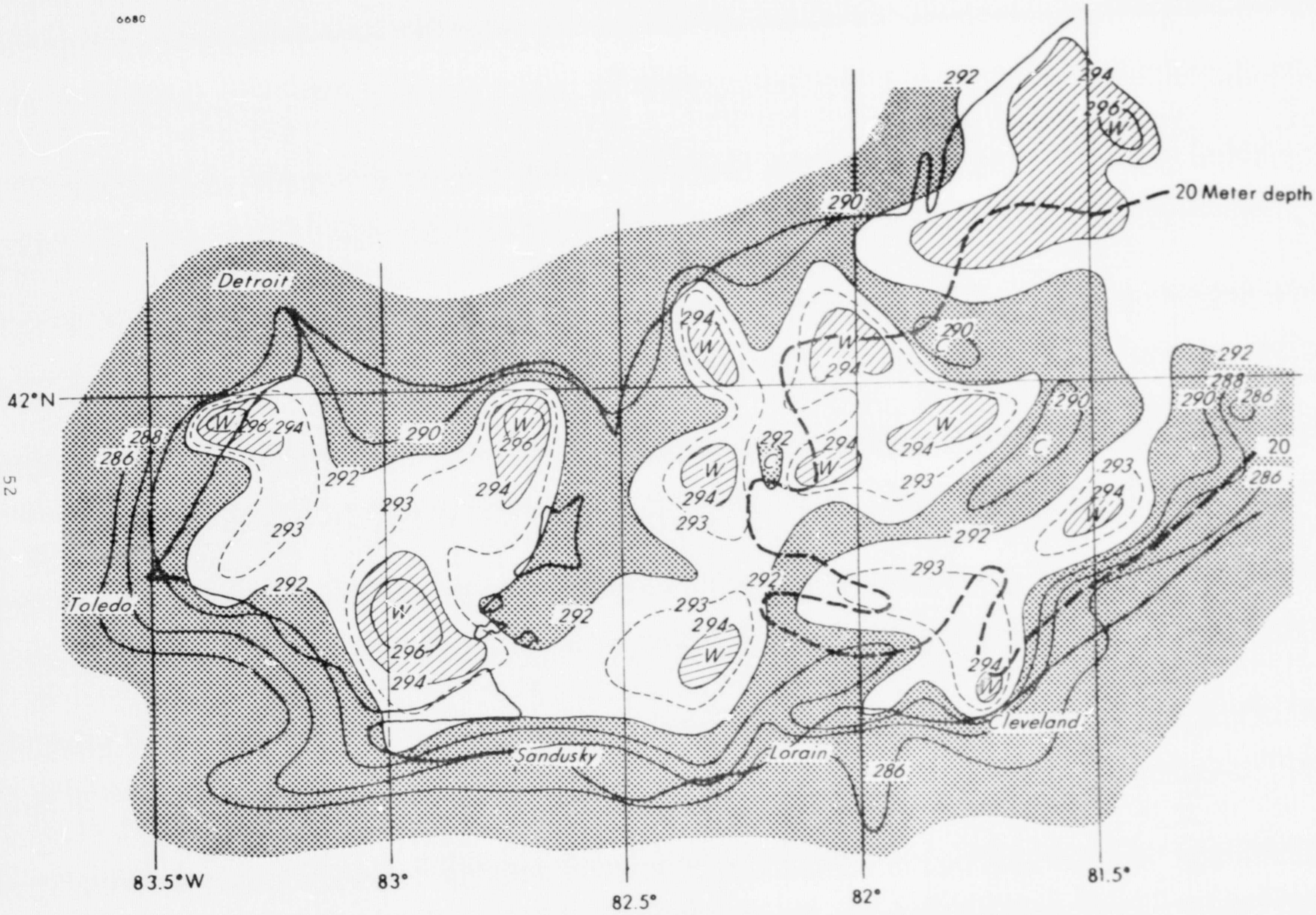

Figure 25 An Example of a Portion of an Analysis of Lake Erie Surface Temperatures Based on Digitized Nimbus II, HRIR. Area was Observed by Nimbus II at Night on 20 August 1966. Temperatures are in Kelvins.

Popham and Samuelson (Ref. 16) found that the HRIR could detect considerable detail in the coastlines and sea ice over the polar regions.

In a study of the meteorological interpretation of the Nimbus HRIR data, Barnes (Ref. 20) found that various broken ice or ice-free areas could be detected by the HRIR in the pack ice region around Antarctica. Some areas appeared gray in the HRIR pictorial data, signifying slightly higher temperatures than the surrounding ice. Those were likely areas of broken ice. Other areas that appeared nearly black (much warmer) were probable ice-free areas. Predoehl (Ref. 17) established boundaries on the Antarctic ice pack from HRIR and from AVCS data.

4. NON-METEOROLOGICAL APPLICATIONS OF FUTURE NIMBUS OBSERVATIONS

The Nimbus B and D satellites, to be launched in 1969 and 1970 respectively will carry new types of scientific and technological experiments that will find many applications to the Earth Resources problems.

Tables 5 and 6 list the proposed experiments for Nimbus B and D and their purposes (Ref. 52). Nimbus E and F, still in the planning stage, are scheduled for the early 1970's (Ref. 53).

Experiments applicable to the Earth Resources Program will briefly be discussed.

4.1 The Nimbus B Satellite

4.1.1 The HRIR Experiment

The HRIR will sense the atmosphere in two spectral bands, 0.7 to 1.3μm for daytime scanning, and 3.4 to 4.2μm for nighttime. The daytime measurements will reveal novel characteristics of the surface through quantitative measurements of its albedo. Vegetation areas, hitherto, difficult to distinguish, will be differentiated with little effort. Vegetation areas will be characterized by relatively high reflectances in the 0.7 to 1.3μm band (Fig. 26 and Ref. 1). A quick comparison with IDCS pictures (taken in the 0.45 to 0.65μm band) will help delineate the suspected areas of vegetation appearing dark (low reflectivities) in the IDCS, from adjacent unvegetated areas also of dark texture.

4.1.2 The IDCS Experiment

The IDCS, because of its greater dynamic range, will produce pictures of improved tonal characteristics over present television pictures such as the AVCS. It will, therefore, be possible to detect terrain features unnoticed in the Nimbus I and II AVCS pictures.

Table 5
Proposed Experiments for Nimbus B

Experiments	Spectral Interval (μm)	Application
Interferometer spectrometer	5-20 (5 cm^{-1})	Atmospheric structure (T, H_2O, O_3, etc)
Satellite infrared spectrometer	15 (5 cm^{-1})	Vertical temperature profile
High resolution infrared radiometer	0.7-1.3	Daytime cloud mapper
	3.4-4.2	Nighttime IR cloud mapper
Medium resolution infrared radiometer	6.7	H_2O mapping-upper atmosphere
	10-11	Surface temperature
	14-16	Stratospheric temperature
	20-23	H_2O mapping-Lower atmosphere
	0.2-4.0	Reflected sunlight
Monitor of ultraviolet solar energy	0.11-0.30	Time variation in solar UV
Image dissector camera	0.45-0.65	Daytime TV cloud mapper
Interrogation, recording and location system	-	Data collection and ranging

Table 6
Proposed Experiments for Nimbus D

Experiments	Spectral Interval (μm)	Application
Interferometer spectrometer	8-40 (2.5 cm^{-1})	Atmospheric structure
Satellite infrared spectrometer	15, 20-40	Temperature and humidity profiles
Filter wedge spectrometer	3-7	Vertical H_2O distribution
Backscatter UV spectrometer	0.25-0.34	Vertical O_3 and total O_3 distribution
Temperature humidity infrared radiometer	10-12	Surface temperature
	6.7	High resolution H_2O mapping
Selective chopper radiometer	15 (1.5 cm^{-1})	Vertical temperature profile
Monitor of UV solar energy	0.11-0.30	Solar UV variation
Image dissector camera	0.45-0.65	Cloud mapper
Interrogation recording and location system	-	Data collection, ranging, and wind tracing

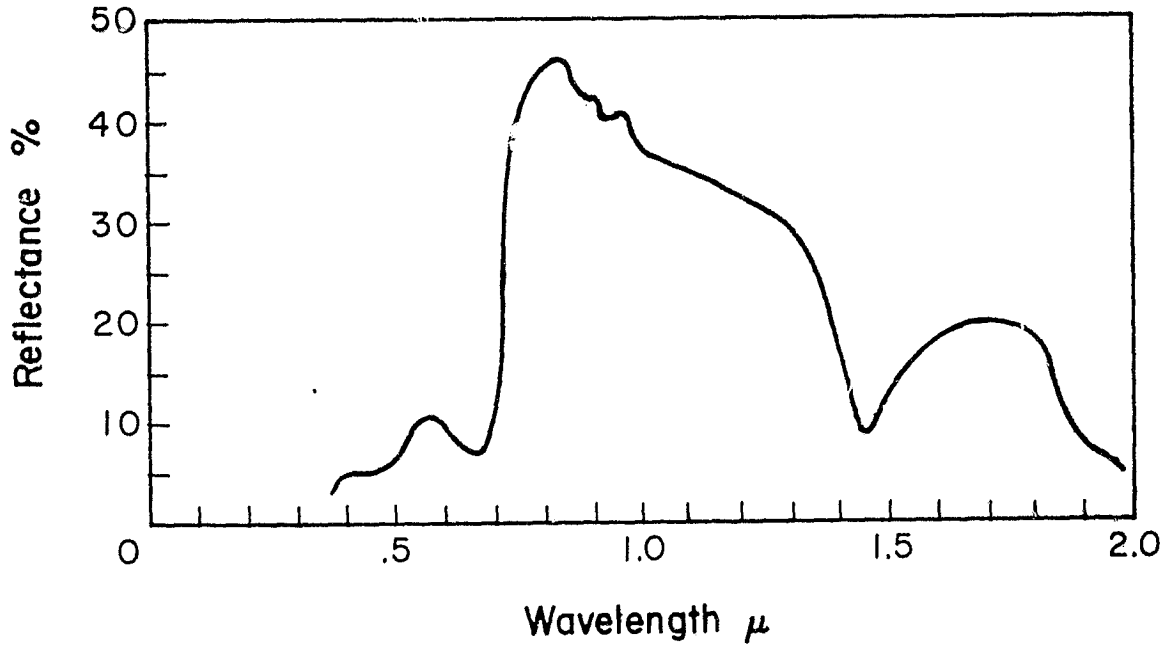

6915

Figure 26 Average Reflectivity for Green Foilage.
From Reference 1, Volume 3.

4.1.3 The IRIS Experiment

The IRIS will provide a spectrum of the sensed radiation between 5 and 20μm with a spectral resolution of 5 cm^{-1} and a ground resolution of about 100 miles. The IRIS experiment's main purpose is to derive vertical temperature pr ;files, and estimate concentration of minor atmospheric gases. The spectrum, with appropriate corrections for the atmospheric constituents, may reveal characteristics due to the surface constitution. It is well known that many rock types have emission minima (reststrahlen minima) between 9 and 11μm (Ref. 54). The position of the minimum, a characteristic signature of the rock sample, varies from about 9μm for acid rocks (for example, 8.8μm for granite) to about 11μm for ultrabasic rocks (for example 10.7μm for dunite, Ref. 55). The difficulty in the detection of some of the minima from satellite heights is the presence of the strong absorption band of atmospheric ozone at 9.6μm (Ref. 37). This limits the recognition of the reststrahlen to few rock types, unless the effects of the O_3 band can be appropriately subtracted.

A measure of the low level O_3 concentration would be indicative of the atmospheric pollution (Ref. 1). Thus, monitoring of pollution over large areas may be possible.

The coarse ground resolution of the IRIS is the greatest drawback in its applications to surface identification. It may nevertheless be possible to establish rough correlations between features in the spectra and ground types of large extent and O_3 atmospheric concentrations. These rough correlations will establish the methodology for future high resolution spectroscopic investigations from space.

4.1.4 The SIRS Experiment

The SIRS experiment will derive atmospheric temperature profiles by measuring atmospheric radiation at various intervals of the 15μm CO_2 band. The basic assumption of the method is the constancy of CO_2 concentration in the atmosphere (approximately three parts per ten thousand per volume). This assumption may be confirmed or revised (over some parts of the world) by the results of the SIRS experiment. CO_2 concentration is important in establishing climatic trends because it affects the heat budget of the world. An increase in CO_2 would cause an increase in the "greenhouse effect" and therefore an increase of the average world temperatures.

4.1.5 The IRLS Experiment

The IRLS ability to gather information from all over the world quickly may find many applications to the Earth Resources Program (Ref. 1). Monitoring of seismic activity in remote parts of the world will be possible. Tsunamis could be quickly detected by buoys and warnings issued in time. A network of buoys over the oceans will be able to relay surface and subsurface temperatures and currents, salinity, plankton concentrations, etc.

4.2 The Nimbus D Satellite

4.2.1 The Temperature Humidity Infrared Radiometer (THIR)

The 10μm band of the THIR will permit day-night monitoring of surface temperatures. This will provide a measure of the diurnal variation of surface temperature which is related to surface type (Fig. 21 and Refs. 42 and 43). Ground resolution for the 10μm band is expected to be approximately 8 km, the same as the HRIR flown on previous Nimbus satellites. The water vapor channel at 6.7μm will have a resolution of about 50 km at the subpoint. This channel will give information on the water vapor content of the atmosphere.

4.2.2 The IRIS Experiment

The IRIS will cover a spectral interval from 8 to 40 μm with a resolution of 2.5 cm^{-1}. Ground resolution will be 100 miles. The increased spectral resolution and spectral range will provide additional diagnostic information on surface composition. A second reststrahlen minimum in the spectral emission of rock is located at 18-25μm (Ref. 54). The absorption in this spectral region is unfortunately influenced by the rotational bands of atmospheric water, thus only over very dry atmosphere (deserts) can the position of this second reststrahlen minimum be of diagnostic utility.

4.2.3 The SIRS Experiment

The SIRS on Nimbus D will have an additional 20-40μm band besides the 15μm band. The main purpose of the 20-40μm band is to survey atmospheric water vapor. Over regions of the world of minimum atmospheric water vapor surface properties may have an effect on the 20-40μm spectrum

4.2.4 The Filter Wedge Spectrometer (FWS) Experiment

The FWS experiment will measure radiation from 3 to 7μm along a continuous strip approximately 100 miles wide under the orbital path. The main purpose of the experiment is to derive vertical water vapor distribution from the radiation measurements although measurements in the 4μm atmospheric window can also be used to interpret surface characteristics.

4.2.5 Other Experiments

The Backscatter Ultraviolet Spectrometer (BUV) will measure atmospheric ozone, which in the lower atmosphere is an indication of pollution.

The Nimbus D will have a more extensive IRLS experiment than the Nimbus B satellite, and will gather all classes of data from fixed and moving platforms useful to the Earth Resources Program.

4.3 Nimbus E and F Satellites

The experiments being considered for Nimbus E and F will include sensing in the microwave region of the electromagnetic spectrum. In the microwave spectrum, scanning radiometers will produce images of emitted radiation from terrain, water surfaces and rain clouds. At wavelengths greater than 1.6 cm radiation is received from depths a few centimeters below the surface and is not appreciably altered by the atmosphere or by non-precipitating clouds. Thus, the nature of land, ice and snow surfaces, and sea state can be mapped and determined more precisely. A radiometer operating at a wavelength of about 1.6 cm and providing a spectral resolution of about 50 km from 1000 km orbit is now under construction. It is expected to be flown in the early 1970's (Refs. 56 and 57).

Supercooled detectors will permit development of spectrometers, interferometers, and infrared radiometers with greatly improved spectral resolutions. Detectors cooled to 25K would permit spectrometer resolution of about 1 km (Ref. 37). A very high resolution infrared radiometer currently under development with a narrow field of view of only 1/2 milliradians would provide a ground resolution of 1/2 km from an orbital altitude of 1000 km.

Television tubes with 10,000 lines resolution will permit from satellite altitudes the ground resolutions presently obtained from aircraft sensors (Ref. 52).

REFERENCES

1. Michigan, University of, 1966: Peaceful Uses of Earth-Observation Spacecraft, Volume 1, "Introduction and Summary," NASA CR-586; Volume 2, "Survey of Applications and Benefits," NASA CR-587; Volume 3, "Sensor Requirements and Experiments," NASA CR-588.

2. Widger, W.K., Jr., P.E. Sherr and C. Rogers, 1964: Practical Interpretation of Meteorological Satellite Data, Final Report, Contract No. AF 19(628)-2471, ARACON Geophysics Company.

3. Widger, W.K., Jr., J.C. Barnes, E.S. Merritt and R.B. Smith, 1966: Meteorological Interpretation of Nimbus HRIR Data, Contract No. 5-9554, Allied Research Associates, Inc.

4. Wark, D.Q., and R.W. Popham, 1962: Ice Photography from the Meteorological Satellites TIROS I and II, Meteorological Satellite Laboratory, Report No. 8, USWB.

5. Wark, D.Q., R.W. Popham, W.A. Dotson, and K.S. Calow, 1962: "Ice Observations by the TIROS II Satellite and by Aircraft," Arctic, 15(1), pp. 9-26.

6. Tarble, R.D., 1963: "Areal Distributions of Snow as Determined from Satellite Photographs," I.A.S.H., 65, pp. 372-375.

7. Cronin, J.F., 1963: Terrestrial Features of the United States as Viewed by TIROS, Scientific Report No. 2, Contract No. AF 19(628)-2471, ARACON Geophysics Company.

8. Merifield, P.M., and J. Rammelkamp, 1964: Terrain in TIROS Pictures, Report No. LR17848, Contract No. NAS 5-3390, Lockheed - California Company.

9. Morrison, A., and B.J. Bird, 1964: "Photography of Earth from Space and Its Non-Meteorological Applications," Proceedings of 3rd Symposium on Remote Sensing of Environment, University of Michigan.

10. Taggert, C.I., 1965: "Interpretation of Geological Features on a Satellite Photograph," Nature, 207, pp. 513-514.

11. National Aeronautics and Space Administration, 1965: Nimbus I Users' Catalog: AVCS and APT, Goddard Space Flight Center.

12. U.S. Geological Survey, 1968: Tectonic Map of the U.S.S.R., compiled and edited by the Geological Survey

13. Woloshin, A.J., 1965: Notes on Geologic Interpretation of Nimbus AVCS Image of Southern California, Geonautics, Inc., Falls Church, Virginia.

14. Chief Topographic Engineer, 1965: "Cartographic and Geologic Uses of Nimbus I AVCS Data," Space Applications, NASA SP-137, pp. 60-61.

15. National Geographic Society, 1963: National Geographic Atlas of the World, Washington, D.C.

16. Popham, R., and R.E. Samuelson, 1965: "Polar Exploration with Nimbus," Observations from the Nimbus I Meteorological Satellite, NASA SP-89, pp. 47-49.

17. Predoehl, M., 1966: "Antarctic Pack Ice: Boundaries Established from Nimbus I Pictures," Science, 153, pp. 861-863.

18. Sissala, J., 1968: Observations of an Antarctic Ocean Tabular Iceberg from the Nimbus II Satellite, Unpublished Paper.

19. U.S. Navy Hydrographic Office, 1957: Oceanographic Atlas of the Polar Seas, (H.O. Pub. No. 75, Reprinted in 1958).

20. Barnes, J.C., and C.J. Bowley, 1966: Snow Cover Distribution as Mapped from Satellite Photography, Final Report, Contract No. Cwb-11269, Allied Research Associates, Inc.

21. Barnes, J.C., and C.J. Bowley, 1968: Operational Guide for Mapping Snow Cover from Satellite Photography, Contract No. E-162-67(N), Allied Research Associates, Inc.

22. Allied Research Associates, Inc., 1967: Proposal to Map Mountain Snow from Satellite Photography, Document No. ARA-4219.

23. Allied Research Associates, Inc., 1967: Proposal for the Study of Northern Hemisphere Terrestrial Features for Satellite Snow Mapping, Document No. ARA-4220.

24. Kunde, V.G., 1965: "Theoretical Relationship Between Equivalent Black Body Temperatures and Surface Temperatures Measured by the Nimbus High Resolution Infrared Radiometer," Observations from the Nimbus I Meteorological Satellite, NASA SP-89, pp. 23-36.

25. Office of Naval Research, 1965: Handbook of Military Infrared Technology, Department of the Navy, Washington, D.C.

26. Hovis, W.A., Jr., 1966: "Infrared Spectral Reflectance of Some Common Minerals," Applied Optics, 5 (2), pp 245-248.

27. Hovis, W.A., Jr., and W.R. Callahan, 1966: "Infrared Reflectance Spectra of Rocks, Tuffs and Red Sandstone from 0.5 to 22 Microns," Journal of the Optical Society of America, 56 (5), pp 639-643.

28. National Aeronautics and Space Administration, 1966: Nimbus II Users'Guide, Goddard Space Flight Center, Greenbelt, Maryland.

29. Kennedy, J.S., 1965: HRIR Noise, Memorandum of 16 April 1965, Goddard Space Flight Center, Greenbelt, Maryland.

30. Greaves, J.R., J.H. Willand and D.T. Chang, 1968: Observations of Sea Surface Temperature Patterns and Their Synoptic Changes Through Optimal Processing of Nimbus II Data, Final Report, Contract No. NASW-1651, Allied Research Associates, Inc.

31. Estoque, M.A. and W.S. Yee, 1963: Air-Earth Interface Characteristics at the Atmospheric Boundary Layer, Contract No. AF 19(604)-7484, Report No. 36, Hawaii Institute of Geophysics.

32. Brunt, D., 1941: Physical and Dynamical Meteorology, 2nd edition, Cambridge University Press, pp. 138-139.

33. Pouquet, J., 1968: "An Approach to the Remote Detection of Earth Resources in Sub-Arid Lands. Terrestrial Features in the Southwest U.S. Derived from Nimbus HRIR Measurements with Field Control," To be published as a NASA Technical Note. Presented to the International Congress of Geology in Prague, Czechoslovakia.

34. Pouquet, J., 1967: Remote Detection of Terrain Features from Nimbus I Radiometer Measurements, NASA Technical Note G-864.

35. Pouquet, J., and E. Raschke, 1968: A Preliminary Study of the Detection of Geomorphological Features Over Northeast Africa by Satellite Radiation Measurements in the Visible and Infrared, to be published as a NASA Tech. Note.

36. Nordberg, W., and R.E. Samuelson, 1965: "Terrestrial Features Observed by the HRIR," Observations from the Nimbus I Meteorological Satellite, NASA SP-89, pp. 37-59.

37. Nordberg, W., 1967: Inference of Properties of the Earth from Satellite Measurements of Infrared Emission, Document X-624-67-408, NASA, Goddard Space Flight Center.

38 Van Lopik, J.R. and L.A. Yarborough, 1966: "Comments on Remote Sensing Needs in Geoscience Engineering and Explorations," Proceedings of the Fourth Symposium on Remote Sensing of Environment, University of Michigan.

39. Estes, J.E., 1966: "Some Geographical Applications of Aerial Infrared Imagery," Proceedings of the Fourth Symposium on Remote Sensing of Environment, University of Michigan.

40. Blanchard, D.C., 1964: "A New Volcanic Island," Oceanus, 10(4), pp. 17-19.

41. Thorarinsson, S., 1967: "The Surtsey Eruption and Related Scientific Work," Polar Record, 13(86), pp. 571-578.

42. Lettau, H., 1951: "Theory of Surface - Temperature and Heat-Transfer Oscillations Near a Level Ground Surface," Trans. Am. Geophys. Union, 32, pp. 189-200.

43. Lenschow, D.H., and J.A. Dutton, 1964: "Surface Temperature Variations Measured from an Airplane Over Several Surface Types," Journal of Applied Meteorology, 3 (1), pp 65-69.

44. Sherr, P., A. Glaser, J. Barnes, and J. Willand, 1968: World-Wide Cloud Cover Distributions for Use in Computer Simulations, Final Report, Contract NAS 8-21040, Allied Research Associates, Inc.

45. Kuers, G., 1968: Interpretation of Daytime Measurements by the Nimbus I and II HRIR, NASA TND-4552.

46. Widger, W.K., Jr., and J.R. Greaves, 1968: Bibliography on the Use of Satellites for Oceanographic Observations, Contract No. NASW-1651, Allied Research Associates, Inc.

47. Allied Research Associates, Inc., 1968: A Proposed Feasibility Study to Estimate the Flushing Time of Lake Erie Utilizing Surface Temperature Information from Satellite-borne Radiometers, Document No. 4228.

48. Raschke, E. and M. Pasternak, 1967: The Global Radiation Balance of the Earth Atmosphere System Obtained from Radiation Data of the Meteorological Satellite Nimbus II, Document X-622-67-383, NASA, Goddard Space Flight Center.

49. Raschke, R., F. Moller, and W.R. Bandeen, 1967: The Radiation Balance of the Earth Atmosphere System Over Both Polar Regions Obtained from Radiation Measurements of the Nimbus II Meteorological Satellite, Document X-622-67-460, NASA, Goddard Space Flight Center.

50. Pasternak, M., 1967: An Atlas of Total Outgoing Long-Wave Radiation and of Short-Wave Reflectance from Nimbus II Observations, Document X-622-67-500, NASA, Goddard Space Flight Center.

51. Allied Research Associates, Inc., 1968: Proposal for Study of the Nimbus HRIR Data for Snow Cover Surveillance, Document ARA-4227.

52. Press, P. and W.B. Huston, 1967: Nimbus Meteorological Satellite Program, Document X-450-67-396, NASA, Goddard Space Flight Center.

53. National Aeronautics and Space Administration, 1967: Summary of the Nimbus Program (Nimbus E and F), Office of Space Science and Applications, Goddard Space Flight Center.

54. Vickers, R.S., and R.J.P. Lyon, 1967: "Infrared Sensing from Spacecraft. A Geological Interpretation," AIAA Thermophysics Specialists Conference, Paper No. 67-284, New Orleans, Louisiana.

55. Lyon, R.J.P. and J.W. Patterson, 1966: "Infrared Spectral Signatures - A Field Geological Tool," Proceedings of the Fourth Symposium on Remote Sensing of Environment, University of Michigan, pp. 215-230.

56. Nordberg, W., 1967: Satellite Studies of the Lower Atmosphere, Document X-620-67-332, NASA, Goddard Space Flight Center.

57. Thaddeus, P., 1966: A Microwave Radiometer for the Nimbus D Meteorological Satellite, Proposal to NASA, GSFC, GISS.

58. Fujita, T. and W. Bandeen, 1965: "Resolution of the Nimbus High Resolution Infrared Radiometer," Journal of Applied Meteorology, 4 (4).